389271-1-T

THE UNIVERSITY OF MICHIGAN

COLLEGE OF ENGINEERING

DEPARTMENT OF ELECTRICAL AND COMPUTER ENGINEERING

Radiation Laboratory

HIGH FREQUENCY SCATTERING BY AN IMPEDANCE DOUBLE WEDGE AND POLYGONAL CYLINDERS

Martin I. Herman and John L. Volakis
Radiation Laboratory
Department of Electrical Engineering and
Computer Science
The University of Michigan
Ann Arbor, Michigan 48109-2122

January, 1987

Northrop Corporation
Aircraft Division
One Northrop Ave.
Hawthorne, CA

389271-1-T = RL-2563

Ann Arbor, Michigan

High Frequency Scattering by an Impedance Double Wedge and Polygonal Cylinders

Martin I. Herman and John L. Volakis

Radiation Laboratory

Department of Electrical Engineering and Computer Science

The University of Michigan

Ann Arbor, Michigan 48109-2122

Abstract-Uniform high frequency diffraction coefficients are presented for up to and including the third order interaction mechanism associated with impedance double wedge structures. Our formulation is based on the Extended Spectral Ray Method and thus rigorously accounts for surface wave contributions. Also key identities are provided that enable the efficient asymptotic evaluation of the resulting integrals via a modified Pauli-Clemmow steepest descent method. Without these identities the derivatives of extremely complicated functions would have to be computed.

Examples of the geometries presented in this report include the thick impedance half plane, the impedance insert in a full plane whose outer faces do not intersect and convex cylindrical polygons composed of multiple double wedge structures.

1 Introduction

Interest in diffraction from material coated structures has prompted the investigation of geometries such as those of impedance strips, thick half planes, polygonal cylinders, and inserts in a full plane. All of the above structures have a generic double wedge structure in which one face is common to both wedges.

Prior work in this area has been for the case of a perfectly conducting double wedge configuration which included only the primary and doubly diffracted mechanisms [1]. In this paper we will present uniform diffraction coefficients up to and including third order mechanisms associated with the impedance double wedge and in which the contribution of the surface waves are rigorously included. The coefficients for the double and triple diffraction mechanisms are derived by using the Extended Spectral Ray Method (ESRM) [2] and thus remain valid even when one edge lies in the transition region of another. Of particular importance in this derivation is the introduction of identities which greatly simplify the Maclaurin series expansion associated with the modified Pauli-Clemmow steepest descent asymptotic evaluation of the integrals. Without these, the evaluation of the derivatives of rather complex functions would be required.

In this report we will consider the isolated double wedge structures shown in figure 1 and also cylindrical structures with a polygonal surface as shown in figure 2. Examples of isolated double impedance wedges are the thick impedance half plane and the impedance insert shown in figures 3 and 4. Some calculations for the scattering by these special structures have recently appeared in the literature [3,4], and are therefore of interest for the purpose of verifying our solution.

In the case of isolated double wedges, all interactions are among two edges. However, when considering the scattering by a polygonal cylinder, our solution is extended to include the contribution of triply diffracted mechanisms which may involve up to three wedge vertices of the polygon. The first of these vertices must, of course, be directly illuminated and the last will be visible to the observer.

Section 2 of this report presents the analysis associated with the isolated double impedance wedge along with backscatter and bistatic calculations of some which are compared to those generated by an alternate formulation. In section 3, the analysis is extended to the case of a polygonal cylinder by accounting for the additional triple diffraction mechanisms. Calculations are also presented for triangular and square cylinders, and are compared with moment method data. Both backscatter and bistatic patterns are presented in order to demonstrate the importance of the multiple interactions.

Finally, section 4 presents the analysis of an impedance strip as a special case of the cylindrical polygon. In this case, however, one must include the contribution of double and triple diffraction mechanisms associated with the bottom surface of the strip. We note that the impedance strip has been considered previously via the ESRM by employing the integral describing the scattering by an impedance half plane as given in [5] . Here the more general representation of the field scattered by an impedance wedge as given by Maliuzhinets [6] is employed, and it is therefore of interest to compare the results generated by the two formulations. They are, of course, expected to be the same.

2 Double Wedge Formulation

The geometry of the isolated double wedge having external wedge angles of $n\pi$ at Q_1 and $m\pi$ at Q_2 is shown in figure 1. In this section only the interactions between the edges at Q_1 and Q_2 will be considered. The resulting solution will therefore be directly applicable to geometries such as the thick impedance half plane and impedance insert. Up to triple diffraction mechanisms will be included in the solution, and it will be seen that these are sufficient to accurately evaluate the scattering by double wedges having a common face of width as small as $\frac{\lambda}{8}$. For the case of the impedance insert, results will be also given which demonstrate the importance of the surface wave interactions at grazing aspects.

Throughout our analysis Q_1 will be our phase reference point and all local angles will be measured with respect to the common ("o") wedge face. In addition, η_0, η_1 and η_2 will respectively denote the normalized impedances of the common face, the outer ("n") face at Q_1 and the outer ("n") face at Q_2 respectively.

2.1 Primary Diffraction from an Impedance Wedge

A plane wave

$$\left.\begin{matrix} E_z^i \\ H_z^i \end{matrix}\right\} = e^{jk(x\cos\phi_o + y\sin\phi_o)} \tag{1}$$

is assumed to be normally incident upon the isolated wedge shown in figure 5. From Maliuzhinets[6] we then find that an integral representation of the diffracted field is (here and in all subsequent references u will represent E_z or H_z)

$$u_1^d(\phi,\phi_o) = \frac{j}{2\pi n} \int_{S(0)} \frac{\sin\frac{\phi_o}{n}}{\Psi(\frac{n\pi}{2}-\phi_o)} e^{-jk\rho\cos\alpha} \cdot \left\{ \frac{\Psi(\alpha+\pi+\frac{n\pi}{2}-\phi)}{\cos(\frac{\alpha+\pi-\phi}{n})-\cos(\frac{\phi_o}{n})} - \frac{\Psi(\alpha-\pi+\frac{n\pi}{2}-\phi)}{\cos(\frac{\alpha-\pi-\phi}{n})-\cos(\frac{\phi_o}{n})} \right\} d\alpha \tag{2}$$

where $S(0)$ is the steepest descent path (see figure 6) obtained after the deformation of the Sommerfeld contour. In addition, ϕ_o is the angle of incidence, ϕ is the observation angle and Ψ is a function defined by Maliuzhinets[6] as

$$\Psi(\alpha) = \Psi_\Phi(\alpha+\Phi+\frac{\pi}{2}-\theta^+)\Psi_\Phi(\alpha-\Phi-\frac{\pi}{2}+\theta^-)\Psi_\Phi(\alpha+\Phi-\frac{\pi}{2}+\theta^+)\Psi_\Phi(\alpha-\Phi+\frac{\pi}{2}-\theta^-) \tag{3}$$

In the above, $\Psi_\Phi(z)$ is usually referred to as the Maliuzhinets function for which highly accurate approximations are given in [7] for all z. Also $\Phi = \frac{n\pi}{2}$ (2Φ is the external wedge angle) and

$$\theta^\pm = \begin{cases} \sin^{-1}(\frac{1}{\eta}) & \text{E-pol.} \\ \sin^{-1}(\eta) & \text{H-pol.} \end{cases}, \tag{4}$$

where the $\pm$ corresponds to the common ("o") and outer ("n") faces of the wedge, respectively.

Equation (2) can be rewritten in a form which is needed when considering the evaluation of the double diffraction integral having a vanishing integrand at the saddle point. Such a form is obtained by introducing the identity

$$\Psi(\alpha+\frac{n\pi}{2}-\pi) = C(\alpha,\theta^+,\theta^-,n)\Psi(\alpha+\frac{n\pi}{2}+\pi), \tag{5}$$

where

$$C = C(\alpha, \theta^+, \theta^-, n) = \frac{\sin(\frac{\alpha-\pi+\theta^+}{2n})\sin(\frac{\alpha-\theta^+}{2n})}{\sin(\frac{\alpha+\pi-\theta^+}{2n})\sin(\frac{\alpha+\theta^+}{2n})} \cdot \frac{\cos(\frac{\alpha-\pi+\theta^-}{2n})\cos(\frac{\alpha-\theta^-}{2n})}{\cos(\frac{\alpha+\pi-\theta^-}{2n})\cos(\frac{\alpha+\theta^-}{2n})}. \tag{6}$$

When (5) is substituted in (2) we obtain

$$u_1^d(\phi, \phi_o) = \frac{j}{2\pi n}\int_{S(0)} e^{-jk\rho\cos\alpha}\sin(\frac{\alpha-\phi}{n})\frac{\Psi(\alpha-\phi+\frac{n\pi}{2}+\pi)}{\Psi(\frac{n\pi}{2}-\phi_o)} \cdot\left\{\frac{1}{\cos(\frac{\pi+\phi_o}{n})-\cos(\frac{\alpha-\phi}{n})} - \frac{1}{\cos(\frac{\pi-\phi_o}{n})-\cos(\frac{\alpha-\phi}{n})} - \frac{\sin(\frac{\phi_o}{n})C_{on}(\alpha-\phi)}{\cos(\frac{\pi-\alpha+\phi}{n})-\cos(\frac{\phi_o}{n})}\right\} d\alpha. \tag{7}$$

In the above, we also made use of the relations

$$C = 1 + (C-1), \tag{8}$$

$$C(\alpha, \theta^+, \theta^-, n) - 1 = \sin(\frac{\alpha}{n})C_o(\alpha, \theta^+, \theta^-, n) = \sin(\frac{\alpha}{n})C_{on}(\alpha), \tag{9}$$

$$C_{on}(\alpha) = \frac{.25\{\sin(\frac{\theta^+}{n}) - \sin(\frac{\theta^-}{n}) - 2\sin(\frac{\pi}{n})\cos(\frac{\alpha}{n}) + \sin(\frac{\pi-\theta^+}{n}) + \sin(\frac{\theta^--\pi}{n})\}}{\sin(\frac{\alpha+\pi-\theta^+}{2n})\sin(\frac{\alpha+\theta^+}{2n})\cos(\frac{\alpha+\pi-\theta^-}{2n})\cos(\frac{\alpha+\theta^-}{2n})} \tag{10}$$

and

$$\frac{\sin(\frac{\phi_o}{n})}{\cos(\frac{\alpha+\pi}{n})-\cos(\frac{\phi_o}{n})} - \frac{\sin(\frac{\phi_o}{n})}{\cos(\frac{\alpha-\pi}{n})-\cos(\frac{\phi_o}{n})} = \sin(\frac{\alpha}{n})\left\{\frac{1}{\cos(\frac{\pi+\phi_o}{n})-\cos(\frac{\alpha}{n})} - \frac{1}{\cos(\frac{\pi-\phi_o}{n})-\cos(\frac{\alpha}{n})}\right\}. \tag{11}$$

The first order asymptotic evaluation of (2) corresponds to the diffracted field from an isolated wedge whose non-uniform form (valid in the far zone) is

$$u_1^d(\phi, \phi_o) = \frac{j}{2\pi n}\sqrt{\frac{2\pi}{k\rho}}e^{-jk\rho}e^{j\frac{\pi}{4}}\frac{\sin\frac{\phi_o}{n}}{\Psi(\frac{n\pi}{2}-\phi_o)}\left[\frac{\Psi(\pi+\frac{n\pi}{2}-\phi)}{\cos(\frac{\pi-\phi}{n})-\cos(\frac{\phi_o}{n})} - \frac{\Psi(-\pi+\frac{n\pi}{2}-\phi)}{\cos(\frac{\pi+\phi}{n})-\cos(\frac{\phi_o}{n})}\right] \tag{12}$$

or from (7)

$$u_1^d(\phi,\phi_o) = \frac{1}{2\pi n}\sqrt{\frac{2\pi}{k\rho}}e^{-jk\rho}e^{-j\frac{\pi}{4}}\sin\frac{\phi}{n}\frac{\Psi(-\phi+\frac{n\pi}{2}+\pi)}{\Psi(\frac{n\pi}{2}-\phi_o)}$$
$$\cdot\left\{\frac{1}{\cos(\frac{\pi+\phi_o}{n})-\cos(\frac{\phi}{n})}-\frac{1}{\cos(\frac{\pi-\phi_o}{n})-\cos(\frac{\phi}{n})}-\frac{\sin(\frac{\phi_o}{n})C_{on}(-\phi)}{\cos(\frac{\pi+\phi}{n})-\cos(\frac{\phi_o}{n})}\right\}$$

Since we are primarily concerned with far field patterns, a uniform primary diffraction coefficient is not required. If we were, however, interested in such a coefficient, then the approach discussed in [8] will be directly applicable for its derivation. We remark that by using this approach, the resulting coefficient will be uniform at the geometrical optics as well as surface wave boundaries.

2.2 Geometrical Optics and Surface Wave Poles

In the subsequent derivation of valid coefficients accounting for the contributions of the double and triple diffraction mechanisms we will require a knowledge of the poles arising in the integrals which render their contribution. These will be the traditional geometrical optics poles and the surface wave poles appearing in the integrands of (2) or (7). The geometrical optics poles are easily identified as the zeros of the trigonometric terms within the brackets. However, the surface wave poles are associated with the Ψ function and can be identified only after using the identity

$$\Psi_\Phi[z\pm(2\Phi+\frac{3\pi}{2})]=\pm\sin\frac{\pi(\pi\pm z)}{4\Phi}\csc(\frac{\pi z}{4\Phi})\Psi_\Phi(2\Phi-\frac{\pi}{2}\pm z). \qquad (13)$$

The pole associated with the surface wave field on the common wedge ("o")

face occurs when the condition

$$\alpha - \Phi - \pi - \theta^+ = 0 \tag{14}$$

is satisfied. This field exists if its associated pole is captured in the deformation of the Sommerfeld contour to the steepest descent path and this occurs when

$$gd(Im(\theta^+)) - Re(\Phi + \pi + \theta^+) > 0, \tag{15}$$

where gd is the Gudermann function and $\Phi + \pi + \theta^+$ is the surface wave pole. We note, however, that even if a surface wave does not exist, surface ray diffraction effects must still be accounted for when considering the multiple diffraction effects as presented next.

2.3 Double Diffraction Mechanism

Starting with the geometry in figure 7, we will explicitly derive the bistatic second order mechanism from Q_1 to Q_2 via the Extended Spectral Ray Method (ESRM) [2] . The integrand of equation (7) may be considered as an infinite sum of complex plane waves which are launched from Q_1 at an angle $-\alpha$. A simple geometrical argument now shows that plane waves forming a local angle $-\alpha$ at Q_1 will form a local angle α at Q_2 as demonstrated in figure 8. Thus, the complex plane wave launched from Q_1 at an angle $-\alpha$ will be incident at Q_2 at an angle α. Clearly, the diffracted field from Q_2 due to a plane wave incident at an angle α and diffracting at an angle ϕ_2 is (see (12b))

$$u_2^d(\alpha,\phi_2) = \frac{1}{2\pi m}\sqrt{\frac{2\pi}{k\rho}}e^{-jk\rho}e^{j\frac{3\pi}{4}}e^{-jkw\cos\alpha}\sin\frac{\phi_2}{m}\frac{\Psi(-\alpha+\frac{m\pi}{2}+\pi)}{\Psi(\frac{m\pi}{2}-\phi_2)}$$
$$\cdot\left\{\frac{1}{\cos(\frac{\pi-\phi_2}{m})-\cos(\frac{\alpha}{m})}-\frac{1}{\cos(\frac{\pi+\phi_2}{m})-\cos(\frac{\alpha}{m})}+\frac{\sin(\frac{\phi_2}{m})C_{om}(-\alpha)}{\cos(\frac{\pi+\alpha}{m})-\cos(\frac{\phi_2}{m})}\right\} \tag{16}$$

after invoking reciprocity and when its phase is referenced to Q_1. In this case w is the width of the common wedge face.

In accordance with the above argument, the basic integral representing the far zone doubly diffracted field from Q_1 to Q_2 is obtained by multiplying the integrand of (7) by (16) to give

$$u_{21}^d(\phi_2,\phi_o) = \frac{-1}{4\pi^2 mn}\sqrt{\frac{2\pi}{k\rho}}e^{-jk\rho}e^{j\frac{\pi}{4}}\frac{1}{\Psi(\frac{n\pi}{2}-\phi_o)\Psi(\frac{m\pi}{2}-\phi_2)}$$
$$\cdot\int_{S(0)}e^{-jkw\cos\alpha}\sin(\frac{\alpha}{n})\sin(\frac{\alpha}{m})\Psi(\alpha+\frac{n\pi}{2}+\pi)\Psi(-\alpha+\frac{m\pi}{2}+\pi)$$
$$\cdot\left\{\frac{1}{\cos(\frac{\pi+\phi_o}{n})-\cos(\frac{\alpha}{n})}-\frac{1}{\cos(\frac{\pi-\phi_o}{n})-\cos(\frac{\alpha}{n})}-\frac{\sin(\frac{\phi_o}{n})C_{on}(\alpha)}{\cos(\frac{\pi-\alpha}{n})-\cos(\frac{\phi_o}{n})}\right\}$$
$$\cdot\left\{\frac{1}{\cos(\frac{\pi-\phi_2}{m})-\cos(\frac{\alpha}{m})}-\frac{1}{\cos(\frac{\pi+\phi_2}{m})-\cos(\frac{\alpha}{m})}+\frac{\sin(\frac{\phi_2}{m})C_{om}(-\alpha)}{\cos(\frac{\pi+\alpha}{m})-\cos(\frac{\phi_2}{m})}\right\}d\alpha. \tag{17}$$

The first term of the asymptotic expansion of this integral about the saddle point is zero. Therefore, we must employ a higher order expansion to obtain an evaluation of the integral. As a result, higher order integrand derivatives must be computed. Such a computation is rather simple for the integrand in (17) because of the appearance of the product of sines. Clearly, this is the primary reason for preferring (7) and (12b) over (2) and (12a).

Equation (17) is in a form suitable for a uniform evaluation via the modified Pauli-Clemmow approach. It is further of importance to note that such an evaluation must account for the presence of the geometrical optics poles as well as the surface wave pole(s). Details of the evaluation can be found in Appendix A of [9]. We find that the doubly diffracted field from Q_1 to Q_2 is

$$\begin{aligned} u_{21}^{d}(\phi_2,\phi_o) &= \frac{-j}{\pi k(mn)^2}\frac{e^{-jkw}}{\sqrt{w}}\frac{e^{-jk\rho}}{\sqrt{\rho}}\frac{\Psi(\frac{n\pi}{2}+\pi)\Psi(\frac{m\pi}{2}+\pi)}{\Psi(\frac{n\pi}{2}-\phi_o)\Psi(\frac{m\pi}{2}-\phi_2)} \\ &\cdot a_1a_2a_3[A\{1-F_{kp}(kwa_1)\}+B\{1-F_{kp}(kwa_2)\}+C\{1-F_{kp}(kwa_3)\}] \\ &\cdot\left\{\frac{1}{1-\cos(\frac{\pi-\phi_o}{n})}-\frac{1}{1-\cos(\frac{\pi+\phi_o}{n})}-\frac{\sin(\frac{\phi_o}{n})C_{on}(0)}{\cos(\frac{\pi}{n})-\cos(\frac{\phi_o}{n})}\right\} \\ &\cdot\left\{\frac{1}{1-\cos(\frac{\pi+\phi_2}{m})}-\frac{1}{1-\cos(\frac{\pi-\phi_2}{m})}+\frac{\sin(\frac{\phi_2}{m})C_{om}(0)}{\cos(\frac{\pi}{m})-\cos(\frac{\phi_2}{m})}\right\}\frac{e^{-jkz}}{2} \end{aligned} \tag{18}$$

where

$$a_1 = 2\cos^2\frac{\phi_o}{2} \tag{19}$$

$$a_2 = 2\cos^2\frac{\phi_2}{2} \tag{20}$$

$$a_3 = 2\sin^2\frac{\theta}{2} \quad (\theta \text{ of common face}) \tag{21}$$

$$A = \frac{-1}{(a_2-a_1)(a_3-a_1)} \tag{22}$$

$$B = \frac{-1}{(a_1-a_2)(a_3-a_2)} \tag{23}$$

$$C = \frac{-1}{(a_1-a_3)(a_2-a_3)} \tag{24}$$

and

$$F_{kp}(z) = 2j\sqrt{z}e^{jz}\int_{\sqrt{z}}^{\infty} e^{-j\tau^2}d\tau \tag{25}$$

is the UTD transition function [10]. When z is complex, the correct choice for the bramch of $\sqrt{z}$ can be more easily defined after relating $F_{kp}(z)$ to the transition function of Clemmow [11] via the relation

$$F_{kp}(z^2) = \pm 2jzF_C(\pm z). \tag{26}$$

where the minus sign is chosen when $\frac{\pi}{4} < \arg(z) < \frac{5\pi}{4}$, and the positive otherwise. Note that the Clemmow transition function satisfies the identity

$$F_C(-z) = \sqrt{z}e^{-j\frac{\pi}{4}}e^{jz^2} - F_C(z), \tag{27}$$

which is essential for maintaining total field continuity. When (27) is employed in (18), u_{21}^d will therefore include the contribution of the surface wave fields. Furthermore, in (18) $x = -w\cos\phi$ and a factor of one half was also included to account for grazing incidence on the common wedge face.

Equation (18) represents the coefficient for the doubly diffracted field when the incident wave impinges first on Q_1 and then diffracts to Q_2. If we were concerned with the reciprocal diffraction mechanism from Q_2 to Q_1, (18) is still valid provided the following substitutions are made : $x \to -w\cos\phi_o$, $\phi_o \to \pi - \phi_o$, $\phi_2 \to \pi - \phi_2$, $m \to n$, and $n \to m$.

2.4 Triple Diffraction Mechanism $\{Q_n \to Q_{n+1} \to Q_n\}$

The ray geometry of the triple diffraction mechanisms to be considered in this section is shown in figure 9.

In accordance with ESRM, an integral representation for the triply diffracted field from Q_1 to Q_2 and back to Q_1 is

$$u^d_{121}(\phi,\phi_o) = \frac{j}{2\pi n}\int_{S(0)} e^{-jkw\cos\alpha}\sin(\frac{\alpha}{n})u^d_{21}(\alpha,\phi_o)\frac{\Psi(\alpha+\frac{n\pi}{2}+\pi)}{\Psi(\frac{n\pi}{2}-\phi)}$$
$$\cdot\left\{\frac{1}{\cos(\frac{\pi+\phi}{n})-\cos(\frac{\alpha}{n})}-\frac{1}{\cos(\frac{\pi-\phi}{n})-\cos(\frac{\alpha}{n})}-\frac{\sin(\frac{\phi}{n})C_{on}(\alpha)}{\cos(\frac{\pi-\alpha}{n})-\cos(\frac{\phi}{n})}\right\}d\alpha \tag{28}$$

where $u^d_{21}(\alpha,\phi_o)$ is the doubly diffracted field incident at Q_1 and is given in (18) with $\rho = w$. We also note that in deriving (28), reciprocity was invoked for the final diffraction at Q_1 toward the far zone point. Therefore, the integrand of (28) can again be interpreted as an infinite sum of complex plane waves incident (diffracted) at Q_1 at a local angle of $-\alpha$ and diffracted (incident) at a local angle ϕ. We note that this choice of $\pm\alpha$ is consistent with our geometrical interpretation illustrated in figure 8.

Replacing u^d_{21} in (28) by (18) (without the 0.5 grazing factor) gives

$$u^d_{121}(\phi,\phi_o) = \Delta\int_{S(0)} e^{-jkw\cos\alpha}\sin(\frac{\alpha}{n})\sin(\frac{\alpha}{m})\frac{\Psi(\alpha+\frac{n\pi}{2}+\pi)}{\Psi(\frac{m\pi}{2}-\alpha)}$$
$$\cdot\left\{\frac{-2\sin\frac{\pi}{m}}{[1-\cos(\frac{\pi+\alpha}{m})][1-\cos(\frac{\pi-\alpha}{m})]}+\frac{C_{om}(0)}{\cos(\frac{\pi}{m})-\cos(\frac{\alpha}{m})}\right\}$$
$$\cdot\left\{\frac{1}{\cos(\frac{\pi+\phi}{n})-\cos(\frac{\alpha}{n})}-\frac{1}{\cos(\frac{\pi-\phi}{n})-\cos(\frac{\alpha}{n})}-\frac{\sin(\frac{\phi}{n})C_{on}(\alpha)}{\cos(\frac{\pi-\alpha}{n})-\cos(\frac{\phi}{n})}\right\}$$
$$\cdot a_2[A\{1-F_{kp}(kwa_1)\}+B\{1-F_{kp}(kwa_2)\}+C\{1-F_{kp}(kwa_3)\}]d\alpha \tag{29}$$

where

$$\Delta = \frac{e^{-jkw}e^{-jk\rho}}{2\pi^2 k(mn)^2 n\sqrt{w\rho}} \frac{\Psi(\frac{n\pi}{2}+\pi)\Psi(\frac{m\pi}{2}+\pi)}{\Psi(\frac{n\pi}{2}-\phi_o)\Psi(\frac{n\pi}{2}-\phi)} a_1 a_3 \cdot \left\{ \frac{1}{1-\cos(\frac{\pi-\phi_o}{n})} - \frac{1}{1-\cos(\frac{\pi+\phi_o}{n})} - \frac{\sin(\frac{\phi_o}{n})C_{on}(0)}{\cos(\frac{\pi}{n})-\cos(\frac{\phi_o}{n})} \right\}. \tag{30}$$

Equation (29) must now be uniformly evaluated via the modified Pauli-Clemmow method of steepest descent while accounting for the presence of the surface wave and geometrical optics poles. The details of this procedure can be found in Appendix B of [9] and the result is

$$\begin{aligned} u^d_{121}(\phi,\phi_o) = {} & \frac{j2\sqrt{2}e^{-j2kw}e^{j\frac{3\pi}{4}}}{(k\pi)^{\frac{3}{2}}w(nm)^3 n} \frac{e^{-jk\rho}}{\sqrt{\rho}} \frac{\Psi^2(\frac{n\pi}{2}+\pi)\Psi(\frac{m\pi}{2}+\pi)}{\Psi(\frac{n\pi}{2}-\phi_o)\Psi(\frac{n\pi}{2}-\phi)\Psi(\frac{m\pi}{2})} \\ & \cdot \frac{a_1 a_3^2 a_4}{a_3-a_4}[A\{1-F_{kp}(kwa_1)\}+B\{1-F_{kp}(kwa_2)\}+C\{1-F_{kp}(kwa_3)\}] \\ & \cdot [F_{kp}(kwa_3)-F_{kp}(kwa_4)] \cdot \frac{e^{-jkx}}{4} \\ & \cdot \left\{ \frac{1}{1-\cos(\frac{\pi-\phi_o}{n})} - \frac{1}{1-\cos(\frac{\pi+\phi_o}{n})} - \frac{\sin(\frac{\phi_o}{n})C_{on}(0)}{\cos(\frac{\pi}{n})-\cos(\frac{\phi_o}{n})} \right\} \\ & \cdot \left\{ \frac{1}{1-\cos(\frac{\pi-\phi}{n})} - \frac{1}{1-\cos(\frac{\pi+\phi}{n})} - \frac{\sin(\frac{\phi}{n})C_{on}(0)}{\cos(\frac{\pi}{n})-\cos(\frac{\phi}{n})} \right\} \\ & \cdot \left\{ \frac{-2\sin\frac{\pi}{m}}{[1-\cos(\frac{\pi}{m})]^2} - \frac{C_{om}(0)}{1-\cos(\frac{\pi}{m})} \right\}, \end{aligned} \tag{31}$$

where a factor of $\frac{1}{4}$ was included to account for grazing on the common wedge face and

$$a_4 = 2\cos^2(\frac{\phi}{2}).$$

Also the value of x is zero when referring to the case of triple diffraction emanating from Q_1, as discussed above.

When considering the contribution of the triply diffracted field emanating from Q_2 as shown in figure 10, (31) is still valid provided the transformations $\phi_o \rightarrow \pi - \phi_o$, $\phi \rightarrow \pi - \phi$, $m \rightarrow n$, and $n \rightarrow m$ are made in addition to setting $x = -w[\cos(\phi) + \cos(\phi_o)]$.

2.5 General Double Wedge Applications

The thick half plane and the impedance insert in a full plane, shown in figures 3 and 4, are two examples of double wedge structures whose outer wedge faces do not intersect.

The thick impedance half plane is composed of a double wedge structure in which both wedges have an external angle of 1.5π. The Maliuzhinets function in this case is given by

$$\Psi_{\frac{3\pi}{4}}(\alpha) = \frac{\cos\left(\frac{\alpha-\pi}{6}\right)\cos\left(\frac{\alpha+\pi}{6}\right)}{\cos^2\left(\frac{\pi}{6}\right)\cos\left(\frac{\pi}{6}\right)}. \tag{32}$$

Figure 11 presents backscatter patterns for the thick perfectly conducting half plane for both E and H incidences. The thickness of the half plane is varied from 0.95λ down to 0.01λ and in all cases we find that the patterns are nearly identical to those presented in [4] where the Angular Spectrum Method (ASM) along with the Generalized Scattering Matrix Formulation (GSMF) was employed. We note that even for a thickness of 0.01λ the two approaches give nearly identical results and particularly for the H incidence where the contribution of the multiply diffracted fields is significant. Bistatic patterns for the perfectly conducting thick half plane are shown in figure 12, again for both polarizations and a similar set of thicknesses as before. The agreement with the ASM-GSMF still holds remarkably

well.

Figure 13 presents backscatter patterns from a thick impedance half plane with E incidence for $\eta(=\eta_o=\eta_1=\eta_2)=.25,\ 4,\ 2+j2$, and $2-j2$ and for various thicknesses ranging from 0.01λ to 0.4λ. Again, all patterns corresponding to the first three impedances are in agreement with those computed via the ASM-GSMF [3] except for some differences corresponding to the case of $\eta=0.25$. We remark that this discrepency is probably due to the inherent approximation associated with the solution given in [3]. Finally, we note that although all face impedances in the above examples were kept the same, our formulation can certainly account for any arbitrary set of face impedances.

The impedance insert in a full plane is a special case of a double wedge configuration composed of two wedges each having external angles of $2\Phi=\pi$. Thus the required Maliuzhinets function in this case is $\Psi_{\frac{\pi}{2}}(z)$ given by

$$\Psi_{\frac{\pi}{2}}(z)=\Psi_{\pi}(z+\pi)\Psi_{\pi}(z-\pi)/[\Psi_{\pi}(\pi)]^2 \tag{33}$$

where $\Psi_{\pi}(z)$ is the corresponding Maliuzhinets function associated with the impedance half plane. A highly accurate approximation for $\Psi_{\pi}(z)$ was found from [12] to be

$$\Psi_{\pi}(z)\approx\begin{cases}1-0.0139z^2 & \mathrm{Im}(z)\leq 4.2\\ 1.05302\left\{\cos\frac{1}{4}(z-j(ln2)\right\}^{\frac{1}{2}}exp\left\{\frac{jz}{2\pi}e^{jz}\right\} & \mathrm{Im}(z)>4.2\end{cases} \tag{34}$$

provided $\mathrm{Re}(z)<\frac{\pi}{2}$; otherwise, the identities

$$\Psi_\pi(z) = \left\{\Psi_\pi(\frac{\pi}{2})\right\}^2 \frac{\cos\left(\frac{z}{4} - \frac{\pi}{8}\right)}{\Psi_\pi(z-\pi)} \tag{35}$$

$$\Psi_\pi(z^*) = \Psi_\pi^*(z)$$

$$\Psi_\pi(-z) = \Psi_\pi(z)$$

must be employed in conjunction with (33). We note that an alternate approximation for $\Psi_\pi(z)$ can also be found in [7], where the given expressions are applicable for all $\Psi_\Phi(z)$.

Just like the thick half plane above, each face of the impedance insert configuration can be defined separately. However, for the examples to be presented, the outer sides of the insert will have equal impedance values. Figure 14 shows a bistatic pattern for an impedance insert in a ground plane with H-incidence. The impedance insert width was 1.6λ and the source was located just over the surface of the ground plane ($\phi_o = 1^o$). The normalized impedances of the insert were $-j.25, j.25$, and .25 and the results compare favorably with the moment method solution as well as a similar high frequency solution given in [13].

Figures 15 and 16 present the effects of varying the outer side impedances while holding the insert impedance constant ($\eta_o = 2 - j1$). In each case three E-incidence patterns are given corresponding to $\eta_1 = \eta_2 = 0.001$, 10, and 1000. We should note, of course, that the same patterns will correspond to H-incidence but with $\eta_1 = \eta_2 = 1000$, 0.1, and 0.001, respectively. The backscatter patterns shown for insert widths of 1λ and 0.5λ reveal that the surface wave interactions are noticeable at grazing aspects for the H-incidence with outer faces almost

perfectly conducting sides ($\eta_1 = \eta_2 = 0.001$). A similar observation also holds for the bistatic patterns given in figure 16 with incidence at 45^o.

3 Cylindrical Polygons

In this section we remove the restriction requiring the outer sides of the double wedge not to intersect. Now the range of the external wedge angles (2Φ) can be such that $1 < m < 2$, $1 < n < 2$ and thus we can consider the scattering by any polygon whose adjacent sides form a convex shape. The strip is a special case of a polygon whose adjacent sides have zero included angles and fits in the general, framework of this analysis. Its scattered field is given later.

In this section we will consider the far-zone scattered field by a polygon which will include the contribution of all primary, double, and triple diffraction mechanisms.

The contribution of the primary and double diffraction mechanisms are the same as discussed in the previous section provided all parameters of the given expressions are applied to the local geometry of each wedge and double wedge forming the polygon. However, the contribution of the triply diffracted fields will include not only that caused by the interaction of two wedge vertices as discussed earlier, but also that due to interactions involving three wedge vertices as illustrated in figure 17. These last mechanisms have not yet been considered and thus expressions for their contribution are developed in the next section. The procedure used is, of course, parallel to that employed for the evaluation of the triply diffracted field associated with two wedge vertices.

3.1 Triple Diffraction Mechanism $\{Q_n \rightarrow Q_{n+1} \rightarrow Q_{n+2}\}$

This triple diffraction ray path is shown in figure 17. An incident wave on Q_n generates spectral waves diffracting at an angle $-\alpha$ and propagating toward Q_{n+1}. Using the same logic as in the double diffraction analysis we can invoke reciprocity and have an incident wave impinge upon Q_{n+1} and diffracted at a local angle α. The field diffracted at Q_{n+1} is, of course, the doubly diffracted field given in (18) . After diffraction from Q_{n+1} a spectral wave may now propagate towards and diffract at Q_{n+2} before returning to the observer. Since we are concerned with the far field we can again invoke reciprocity and have an incident wave impinge upon Q_{n+2} at an angle ϕ, which will in sequence generate spectral waves diffracted at an angle $-\alpha$. Finally, the spectral waves will impinge at Q_{n+1} at a local angle α or $2\Phi - \alpha$ depending on the chosen face of reference. Thus an integral representation for the triply diffracted field is

$$u^d_{121}(\phi,\phi_o) = \frac{j}{2\pi p} \int_{S(0)} e^{-jkw\cos\alpha} \sin(\frac{\alpha}{p}) u^d_{21}(2\Phi-\alpha,\phi_o) \frac{\Psi(\alpha+\frac{p\pi}{2}+\pi)}{\Psi(\frac{p\pi}{2}-\phi)} \cdot \left\{ \frac{1}{\cos(\frac{\pi+\phi}{p})-\cos(\frac{\alpha}{p})} - \frac{1}{\cos(\frac{\pi-\phi}{p})-\cos(\frac{\alpha}{p})} - \frac{\sin(\frac{\phi}{p})C_{op}(\alpha)}{\cos(\frac{\pi-\alpha}{p})-\cos(\frac{\phi}{p})} \right\} d\alpha \tag{36}$$

where $p\pi$ is the external wedge angle at (Q_{n+2}) while, as before, $n\pi$ and $m\pi$ correspond to the external wedge angles at the first (Q_n) and second (Q_{n+1}) vertices, respectively. We further note that in the above, $u^d_{21}(\alpha,\phi_o)$ is given in (18) .

Substituting for u_{21}^d gives

$$
\begin{aligned}
u_{121}^d(\phi,\phi_o) \;=\; & \Delta \int_{S(0)} e^{-jkw_2\cos\alpha} \sin(\frac{\alpha}{p}) \sin(\frac{\alpha}{m}) \frac{\Psi(\alpha+\frac{p\pi}{2}+\pi)}{\Psi(-\frac{m\pi}{2}+\alpha)} \\
& \cdot \left\{ \frac{-2\sin\frac{\pi}{m}}{[1-\cos(\frac{\pi-\alpha+m\pi}{m})][1-\cos(\frac{\pi-m\pi+\alpha}{m})]} + \frac{C_{om}(0)}{\cos(\frac{\pi}{m})-\cos(\frac{m\pi-\alpha}{m})} \right\} \\
& \cdot \left\{ \frac{1}{\cos(\frac{\pi+\phi}{p})-\cos(\frac{\alpha}{p})} - \frac{1}{\cos(\frac{\pi-\phi}{p})-\cos(\frac{\alpha}{p})} - \frac{\sin(\frac{\phi}{p})C_{op}(\alpha)}{\cos(\frac{\pi-\alpha}{p})-\cos(\frac{\phi}{p})} \right\} \\
& \cdot a_2[A\{1-F_{kp}(kw_1a_1)\}+B\{1-F_{kp}(kw_1a_2)\}+C\{1-F_{kp}(kw_1a_3)\}]d\alpha
\end{aligned}
\tag{37}
$$

where

$$
\begin{aligned}
\Delta \;=\; & \frac{e^{-jkw_1}e^{-jk\rho}}{2\pi^2k(mn)^2p\sqrt{w_1\rho}} \frac{\Psi(\frac{n\pi}{2}+\pi)\Psi(\frac{m\pi}{2}+\pi)}{\Psi(\frac{n\pi}{2}-\phi_o)\Psi(\frac{p\pi}{2}-\phi)} a_1a_3 \\
& \cdot \left\{ \frac{1}{1-\cos(\frac{\pi-\phi_o}{n})} - \frac{1}{1-\cos(\frac{\pi+\phi_o}{n})} - \frac{\sin(\frac{\phi_o}{n})C_{on}(0)}{\cos(\frac{\pi}{n})-\cos(\frac{\phi_o}{n})} \right\}.
\end{aligned}
\tag{38}
$$

Equation (37) can now be uniformly evaluated using the modified Pauli-Clemmow method of steepest descent while accounting for the presence of the surface wave and geometrical optics poles. The result is

$$
\begin{aligned}
u^d_{121} \;=\; & \frac{j2\sqrt{2}e^{-jk(w_1+w_2)}e^{j\frac{3\pi}{4}}}{(k\pi)^{\frac{3}{2}}\sqrt{w_1w_2}(nm)^2p^2m}\,\frac{e^{-jk\rho}}{\sqrt{\rho}}\,\frac{\Psi(\frac{n\pi}{2}+\pi)\Psi(\frac{m\pi}{2}+\pi)\Psi(\frac{p\pi}{2}+\pi)}{\Psi(\frac{n\pi}{2}-\phi_o)\Psi(\frac{p\pi}{2}-\phi)\Psi(-\frac{m\pi}{2})} \\
& \cdot\frac{a_1a_3a_5a_4}{a_5-a_4}[A\{1-F_{kp}(kw_1a_1)\}+B\{1-F_{kp}(kw_1a_2)\}+C\{1-F_{kp}(kw_1a_3)\}] \\
& \cdot[F_{kp}(kw_2a_5)-F_{kp}(kw_2a_4)]\cdot\frac{e^{-jkx}}{4} \\
& \cdot\left\{\frac{1}{1-\cos(\frac{\pi-\phi_o}{n})}-\frac{1}{1-\cos(\frac{\pi+\phi_o}{n})}-\frac{\sin(\frac{\phi_o}{n})C_{on}(0)}{\cos(\frac{\pi}{n})-\cos(\frac{\phi_o}{n})}\right\} \\
& \cdot\left\{\frac{1}{1-\cos(\frac{\pi-\phi}{p})}-\frac{1}{1-\cos(\frac{\pi+\phi}{p})}-\frac{\sin(\frac{\phi}{p})C_{op}(0)}{\cos(\frac{\pi}{p})-\cos(\frac{\phi}{p})}\right\} \\
& \cdot\left\{\frac{-2\sin\frac{\pi}{m}}{[1-\cos(\frac{\pi+m\pi}{m})][1-\cos(\frac{\pi-m\pi}{m})]}+\frac{C_{om}(0)}{1+\cos(\frac{\pi+m\pi}{m})}\right\} \qquad (39)
\end{aligned}
$$

where

$$a_5 = 2\sin^2(\frac{\theta_{n+1}}{2}),$$

in which θ_{n+1} is associated with the surface connecting Q_{n+1} and Q_{n+2}. In addition $x = -w_2'\cos(\phi) - w_1'\cos(\phi_o)$ with ϕ, ϕ_o, w_1', and w_2' as defined in figure 18.

3.2 Cylindrical Polygon Application

In this section we will explore the accuracy of the previously developed coefficients. Particularly, the sum of the contributions from all possible first, second, and triple order mechanisms will be used in predicting the scattered field by impedance polygons. The results will then be compared with corresponding moment method data. It is, of course, expected that as the sides of the polygon become smaller, the higher order mechanisms will become more significant and therefore the accuracy of our third order solution will decrease when fourth order

mechanisms are of importance. The examples considered in this section are the triangular and square cylinders whose sides have equal length and impedances. Their geometries are shown in figure 19.

Backscatter patterns are presented in figure 20 for the triangular cylinder whose sides vary from 1λ down to 0.25λ. These pattern are with E-incidence and correspond to either $\eta = 2 + j2$ (inductive) or $\eta = 2 - j2$ (capacitive). As seen, our high frequency solution agrees remarkably well with the moment method for cylindrical sides as small as $\frac{\lambda}{4}$.

A set of bistatic patterns were also calculated and compared with moment method results. The conclusions are similar to those given for the backscatter case. It is also important to note that in these examples an edge of the cylinder may lie in the non-ray optical region of another edge. In such a situation the diffraction coefficients generated via the ESRM approach are still valid, where as those obtained via the self consistent GTD method [14] would not be applicable.

The backscatter patterns shown in figure 21 correspond to a square cylinder with a normalized impedance of $\eta = 4$, side length of 1λ and E-incidence. A mechanism to mechanism comparison reveals that the backscatter pattern is primarily a first order effect. However, for bistatic cases in which the direction of incidence is almost parallel with a face of the square, the higher order terms are significant. This is illustrated in figure 22 along with moment method results. The pattern due to primary diffraction matches the moment method data only near the backscatter direction. It is further seen to have several discontinuities most of which are compensated only after inclusion of the double diffraction

effects. The rest of the discontinuities are associated with the triple diffraction mechanisms and particularly those involving three vertices. Thus, they are seen to vanish when the triply diffracted field is also included.

We conclude that overall, the agreement of our analytic solution with the moment method data is quite remarkable. Furthermore, although the considered polygons had equal impedances on all sides, it should be noted that our formulation is applicable for any polygon with arbitrary side impedances.

4 Impedance Strip $m = n = 2$

The impedance strip is a special case of the polygonal cylinder (both wedges have $\Phi = 2\pi$) and is included here for completeness purposes. The scattered field by an impedance strip has been previously found via the ESRM using the current spectra of an impedance half plane [15].

For a strip there exist four double diffraction mechanisms and eight triple mechanisms as shown in figures 23 and 24 . Fortunately, we need to only solve for the contribution of two double diffraction and four triple diffraction mechanisms. The contributions of the other mechanisms can then be obtained by an appropriate transformation of the geometrical variables.

4.1 Double Diffraction From a Strip

Let us first consider the diffraction coefficients associated with the double diffraction mechanisms from Q_1 to Q_2. As discussed above, the coefficients associated with the mechanisms from Q_2 to Q_1 can be then found by an appropriate variable transformation. The contribution of the double diffraction mechanism

for the top surface is given by (18), and is still applicable for the strip provided we set $n = m = 2$. However, in the case of the impedance strip, the field due to the double diffraction mechanism associated with the bottom surface must also be accounted for. The procedure in deriving this doubly diffracted field via the ESRM is very similar to that employed in association with the top surface. Some care, though, must be exercised in the definition of the local angles corresponding to the spectral plane waves. Particularly, if we use the bottom ("n") face of the strip as our reference, then the spectral waves in the integral of (2) must be interpreted as forming an angle of α with respect to the bottom face at Q_1. Consequently, they will be forming an angle of -α with the bottom strip face at Q_2. Accordingly, we find that

$$\begin{aligned} u_{21}^{d}(\phi_2,\phi_o) &= \frac{-j}{16\pi k}\frac{e^{-jkw}}{\sqrt{w}}\frac{e^{-jk\rho}}{\sqrt{\rho}}\frac{[\Psi(0)]^2}{\Psi(\pi-\phi_o)\Psi(\pi-\phi_2)} \\ &\cdot a_1 a_2 a_3'[A'\{1-F_{kp}(kwa_1)\}+B'\{1-F_{kp}(kwa_2)\}+C'\{1-F_{kp}(kwa_3')\}] \\ &\cdot\left\{\frac{1}{1+\sin(\frac{\phi_o}{2})}-\frac{1}{1-\sin(\frac{\phi_o}{2})}+\frac{\sin(\frac{\phi_o}{2})C_{2n}(0)}{\cos(\frac{\phi_o}{2})}\right\} \\ &\cdot\left\{\frac{1}{1-\sin(\frac{\phi_2}{2})}-\frac{1}{1+\sin(\frac{\phi_2}{2})}-\frac{\sin(\frac{\phi_2}{2})C_{2m}(0)}{\cos(\frac{\phi_2}{2})}\right\}\frac{e^{-jkz}}{2} \end{aligned} \tag{40}$$

where

$$C_2(\alpha,\theta^+,\theta^-,n)-1=\sin\frac{\alpha}{n}C_{2n}(\alpha), \tag{41}$$

$$C_{2n}(\alpha) = -.25\left\{\frac{\sin(\frac{\theta^+}{n})-\sin(\frac{\theta^-}{n})-2\sin(\frac{\pi}{n})\cos(\frac{\alpha-2\pi}{n})+\sin(\frac{\pi-\theta^+}{n})+\sin(\frac{\theta^--\pi}{n})}{\sin(\frac{\alpha-\pi-\theta^+}{2n})\sin(\frac{\alpha+\theta^+-2\pi}{2n})\cos(\frac{\alpha-\pi-\theta^-}{2n})\cos(\frac{\alpha-2\pi+\theta^-}{2n})}\right\}, \tag{42}$$

$$a_3'=2\sin^2(\frac{\theta^-}{2}), \tag{43}$$

and

$$
\begin{aligned}
A' &= \frac{-1}{(a_2 - a_1)(a_3' - a_1)} \\
B' &= \frac{-1}{(a_1 - a_2)(a_3' - a_2)} \\
C' &= \frac{-1}{(a_1 - a_3')(a_2 - a_3')}
\end{aligned}
$$

Once again, x is equal to $-w\cos\phi$, and a factor of one-half is included to account for grazing effects.

All together there are four double diffraction mechanisms for the strip and the coefficients presented above are for the incident wave impinging upon Q_1 first. If we were concerned with diffraction from Q_2 to Q_1 then we would make the following transformations in (18) and (40) : $x \to -w\cos\phi_o$, $\phi_o \to \pi - \phi_o$ and $\phi_2 \to \pi - \phi_2$.

4.2 Triple Diffraction from a Strip

The eight triple diffraction mechanisms are paired in groups of two as shown in figure 24. Each pair has the same itenerary but in reciprocal directions. The contribution of the triple diffraction mechanisms shown in figure 24(a) is given by (31). Normally we would just list the results for the next three sets of mechanisms if the derivations were the same as those shown in figure 24(a). Unfortunately, this is not the case at hand. Particularly, we must consider the fact that the diffracted field wraps around the strip for the mechanisms in figure 24(c) and (d). Thus, for the sake of completeness the diffracted fields due to the rest of the mechanisms will be derived next.

Starting with the mechanisms in figure 24(b), the integral for the corresponding triply diffracted field is

$$u^d_{121}(\phi,\phi_o) = \frac{j}{4\pi}\int_{S(0)} e^{-jk\rho\cos\alpha}\sin(\frac{\phi}{2})u^d_{21}(2\pi+\alpha,\phi_o) \left[\frac{\Psi(\alpha)}{\sin(\frac{\alpha}{2})-\cos(\frac{\phi}{2})}+\frac{\Psi(-2\pi+\alpha)}{\sin(\frac{\alpha}{2})+\cos(\frac{\phi}{2})}\right]d\alpha \tag{44}$$

where u^d_{21} is defined in (40). Equation (44) can be again interpreted as an infinite sum of spectral plane waves forming an angle α with the bottom face at Q_1 . The angles in u^d_{21} are, of course, defined with respect to the top surface and to be consistent the spectral waves make an angle of $-\alpha$ with the bottom face at Q_2. Inserting (40) into (44) gives

$$\begin{aligned} u^d_{121}(\phi,\phi_o) = {} & \Delta\int_{S(0)} e^{-jkw\cos\alpha}\sin(\frac{\alpha}{2})\sin(\frac{\alpha}{2})\frac{\Psi(\alpha)}{\Psi(-\pi-\alpha)} \\ & \cdot\left\{\frac{2}{\cos^2(\frac{\alpha}{2})}+\frac{C_{2m}(0)}{\cos(\frac{\alpha}{2})}\right\} \\ & \cdot\left\{\frac{1}{\sin(\frac{\phi}{2})-\cos(\frac{\alpha}{2})}+\frac{1}{\sin(\frac{\phi}{2})+\cos(\frac{\alpha}{2})}+\frac{\sin(\frac{\phi}{2})C_{2n}(\alpha)}{\sin(\frac{\alpha}{2})+\cos(\frac{\phi}{2})}\right\} \\ & \cdot a_2[A'\{1-F_{kp}(kwa_1)\}+B'\{1-F_{kp}(kwa_2)\}+C'\{1-F_{kp}(kwa'_3)\}]d\alpha \end{aligned} \tag{45}$$

where

$$\begin{aligned} \Delta = {} & \frac{e^{-jkw}e^{-jk\rho}}{64\pi^2k\sqrt{w\rho}}\frac{\Psi(0)\Psi(2\pi)}{\Psi(\pi-\phi_o)\Psi(\pi-\phi)}a_1a'_3 \\ & \cdot\left\{\frac{1}{1+\sin(\frac{\phi_o}{2})}-\frac{1}{1-\sin(\frac{\phi_o}{2})}+\frac{\sin(\frac{\phi_o}{2})C_{2n}(0)}{\cos(\frac{\phi_o}{2})}\right\} \end{aligned} \tag{46}$$

Finally, by using the modified Pauli-Clemmow approach, (45) yields

$$
\begin{aligned}
u^d_{121}(\phi,\phi_o) \;=\; & \frac{\sqrt{2}e^{-j2kw}e^{j\frac{\pi}{4}}}{64(k\pi)^{\frac{3}{2}}w}\frac{e^{-jk\rho}}{\sqrt{\rho}}\frac{[\Psi(0)]^2\Psi(2\pi)}{\Psi(\pi-\phi_o)\Psi(\pi-\phi)\Psi(-\pi)} \\
& \cdot\frac{a_1 a_3'^2 a_4}{a_3'-a_4}[A'\{1-F_{kp}(kwa_1)\}+B'\{1-F_{kp}(2kw)\}+C'\{1-F_{kp}(kwa_3')\}] \\
& \cdot[F^{\circ}_{kp}(kwa_3')-F_{kp}(kwa_4)]\cdot\frac{1}{4}e^{-jkx} \\
& \cdot\left\{\frac{1}{1+\sin(\frac{\phi_o}{2})}-\frac{1}{1-\sin(\frac{\phi_o}{2})}+\frac{\sin(\frac{\phi_o}{2})C_{2n}(0)}{\cos(\frac{\phi_o}{2})}\right\} \\
& \cdot\left\{\frac{1}{1+\sin(\frac{\phi}{2})}-\frac{1}{1-\sin(\frac{\phi}{2})}+\frac{\sin(\frac{\phi}{2})C_{2n}(0)}{\cos(\frac{\phi}{2})}\right\} \\
& \cdot\{2+C_{2m}(0)\} \qquad (47)
\end{aligned}
$$

where $x = 0$ if the diffraction occurs from Q_1 and $x = -w[\cos(\phi)+\cos(\phi_o)]$ if the diffraction occurs from Q_2.

Continuing our derivation for the contribution of the mechanisms in figure 24(c). Let us first consider the mechanism which initially diffracts along the top face of the strip before wrapping around the bottom face. Using reciprocity, the triple diffraction integral for this case will consist of spectral plane waves diffracting at Q_1 at an angle α. Thus, they will be forming an angle -α with respect to the bottom face at Q_2. As a result the triple diffraction integral for this case is

$$
\begin{aligned}
u^d_{121}(\phi,\phi_o) \;=\; & \frac{j}{4\pi}\int_{S(0)} e^{-jkw\cos\alpha}\sin\frac{\phi}{2}u^d_{21}(2\pi+\alpha,\phi_o) \\
& \cdot\left[\frac{\Psi(\alpha)}{\sin(\frac{\alpha}{2})-\cos(\frac{\phi}{2})}+\frac{\Psi(-2\pi+\alpha)}{\sin(\frac{\alpha}{2})+\cos(\frac{\phi}{2})}\right]d\alpha. \qquad (48)
\end{aligned}
$$

where u^d_{21} is the doubly diffracted field given in (18) with $\rho = w$. Inserting (18)

and (8)-(11) in (48) gives

$$u^d_{121}(\phi,\phi_o) = \Delta\int_{S(0)} e^{-jkw\cos\alpha}\sin(\frac{\alpha}{2})\sin(\frac{\alpha}{2})\frac{\Psi(\alpha)}{\Psi(-\pi-\alpha)}\left\{\frac{2}{\cos^2(\frac{\alpha}{2})}-\frac{C_{om}(0)}{\cos(\frac{\alpha}{2})}\right\}$$
$$\cdot\left\{\frac{1}{\sin(\frac{\phi}{2})-\cos(\frac{\alpha}{2})}+\frac{1}{\sin(\frac{\phi}{2})+\cos(\frac{\alpha}{2})}+\frac{\sin(\frac{\phi}{2})C_{2n}(\alpha)}{\sin(\frac{\alpha}{n})+\cos(\frac{\phi}{2})}\right\}$$
$$\cdot a_2[A\{1-F_{kp}(kwa_1)\}+B\{1-F_{kp}(kwa_2)\}+C\{1-F_{kp}(kwa_3)\}]d\alpha \tag{49}$$

where

$$\Delta = \frac{e^{-jkw}e^{-jk\rho}}{64\pi^2k\sqrt{w\rho}}\frac{[\Psi(2\pi)]^2}{\Psi(\pi-\phi_o)\Psi(\pi-\phi)}a_1a_3$$
$$\cdot\left\{\frac{1}{1-\sin(\frac{\phi_o}{2})}-\frac{1}{1+\sin(\frac{\phi_o}{2})}+\frac{\sin(\frac{\phi_o}{2})C_{on}(0)}{\cos(\frac{\phi_o}{2})}\right\} \tag{50}$$

and

$$a_3=\sin^2(\frac{\theta^+}{2}) \tag{51}$$

A subsequent modified Pauli-Clemmow evaluation of (49) yields

$$u^d_{121}(\phi,\phi_o) = \frac{j\sqrt{2}e^{-j2kw}e^{j\frac{3\pi}{4}}}{64(k\pi)^{\frac{3}{2}}w}\frac{e^{-jk\rho}}{\sqrt{\rho}}\frac{\Psi(0)[\Psi(2\pi)]^2}{\Psi(\pi-\phi_o)\Psi(\pi-\phi)\Psi(-\pi)}$$
$$\cdot\frac{a_1a_3a_3'a_4}{a_3'-a_4}[A\{1-F_{kp}(kwa_1)\}+B\{1-F_{kp}(2kw)\}+C\{1-F_{kp}(kwa_3)\}]$$
$$\cdot[F_{kp}(kwa_3')-F_{kp}(kwa_4)]\cdot\frac{1}{4}e^{-jkx}$$
$$\cdot\left\{\frac{1}{1-\sin(\frac{\phi_o}{2})}-\frac{1}{1+\sin(\frac{\phi_o}{2})}+\frac{\sin(\frac{\phi_o}{2})C_{on}(0)}{\cos(\frac{\phi_o}{2})}\right\}$$
$$\cdot\left\{\frac{1}{1+\sin(\frac{\phi}{2})}-\frac{1}{1-\sin(\frac{\phi}{2})}+\frac{\sin(\frac{\phi}{2})C_{2n}(0)}{\cos(\frac{\phi}{2})}\right\}$$
$$\cdot\{2-C_{om}(0)\}. \tag{52}$$

where $x = 0$ if the final diffraction occurs at Q_1 as developed above and $x = -w[\cos(\phi) + \cos(\phi_o)]$ if the final diffraction is at Q_2.

Finally, the last set of triple diffraction mechanisms to be considered is shown in figure 24(d). This situation is, of course, very similar to the pair of mechanisms in figure 24(c) whose contribution is given by (52). Let us first consider the mechanism which involves first diffraction along the bottom surface and then over the top surface. In this case the triple diffraction integral will consist of spectral plane waves diffracting from Q_1 at an angle of -α with the top surface if reciprocity is involved. Thus, they will be forming an angle of α with respect to the top face at Q_2. As a result the triple diffraction integral will be

$$\begin{aligned} u^d_{121}(\phi,\phi_o) &= \Delta \int_{S(0)} e^{-jkw\cos\alpha} \sin(\frac{\alpha}{2}) \sin(\frac{\alpha}{2}) \frac{\Psi(\alpha+2\pi)}{\Psi(\pi-\alpha)} \\ &\cdot \left\{ \frac{2}{\cos^2(\frac{\alpha}{2})} - \frac{C_{2m}(0)}{\cos(\frac{\alpha}{2})} \right\} \\ &\cdot \left\{ \frac{1}{-\sin(\frac{\phi}{2}) - \cos(\frac{\alpha}{2})} - \frac{1}{\sin(\frac{\phi}{2}) - \cos(\frac{\alpha}{2})} - \frac{\sin(\frac{\phi}{2}) C_{on}(\alpha)}{\sin(\frac{\alpha}{2}) - \cos(\frac{\phi}{2})} \right\} \\ &\cdot a_2 [A'\{1 - F_{kp}(kwa_1)\} + B'\{1 - F_{kp}(kwa_2)\} + C'\{1 - F_{kp}(kwa'_3)\}] d\alpha \end{aligned} \tag{53}$$

where

$$\begin{aligned} \Delta &= \frac{e^{-jkw} e^{-jk\rho}}{64\pi^2 k\sqrt{w\rho}} \frac{[\Psi(0)]^2}{\Psi(\pi-\phi_o)\Psi(\pi-\phi)} a_1 a'_3 \\ &\cdot \left\{ \frac{1}{1+\sin(\frac{\phi_o}{2})} - \frac{1}{1-\sin(\frac{\phi_o}{2})} + \frac{\sin(\frac{\phi_o}{2}) C_{2n}(0)}{\cos(\frac{\phi_o}{2})} \right\} \end{aligned} \tag{54}$$

and we have employed the doubly diffracted field u^d_{21} given in (40). Evaluating

(53) via the modified Pauli-Clemmow approach gives

$$
\begin{aligned}
u^d_{121}(\phi,\phi_o) \;=\; & \frac{j\sqrt{2}e^{-j2kw}e^{j\frac{3\pi}{4}}}{64(k\pi)^{\frac{3}{2}}w}\,\frac{e^{-jk\rho}}{\sqrt{\rho}}\,\frac{[\Psi(0)]^2\Psi(2\pi)}{\Psi(\pi-\phi_o)\Psi(\pi-\phi)\Psi(\pi)} \\
& \cdot\frac{a_1 a_3 a_3^{'} a_4}{a_3^{'}-a_4}[A^{'}\{1-F_{kp}(kwa_1)\}+B^{'}\{1-F_{kp}(kwa_2)\}+C^{'}\{1-F_{kp}(kwa_3^{'})\}] \\
& \cdot[F_{kp}(kwa_3^{'})-F_{kp}(kwa_4)]\cdot\frac{1}{4}e^{-jkx} \\
& \cdot\left\{\frac{1}{1+\sin(\frac{\phi_o}{2})}-\frac{1}{1-\sin(\frac{\phi_o}{2})}+\frac{\sin(\frac{\phi_o}{2})C_{2n}(0)}{\cos(\frac{\phi_o}{2})}\right\} \\
& \cdot\left\{\frac{1}{1-\sin(\frac{\phi}{2})}-\frac{1}{1+\sin(\frac{\phi}{2})}+\frac{\sin(\frac{\phi}{2})C_{on}(0)}{\cos(\frac{\phi}{2})}\right\} \\
& \cdot\{2-C_{2m}(0)\} \qquad (55)
\end{aligned}
$$

for the mechanisms in figure 24(d) where $x = 0$ if the final diffraction occurs at Q_1 and $x = -w[\cos(\phi)+\cos(\phi_o)]$ if the final diffraction is at Q_2. The transformations listed in the double diffraction for a strip apply in this situation to recover the components whose incident field is at Q_2. They are: $\phi_o \rightarrow \pi - \phi_o$ and $\phi \rightarrow \pi - \phi$.

4.3 Comments on the Impedance Strip

The diffracted fields given above for the impedance strip are identical [15] to those derived by employing the half plane diffraction integral given by Senior [5]. The last has, of course, been verified to agree with moment method scattering data for strip widths down to $\frac{\lambda}{8}$ in the case of backscattering. However, the high frequency results generated here by employing the Maliuzhinets impedance wedge diffraction integral along with the ESRM, have the added advantage of allowing non-equal impedances on the top and bottom sides of the strip.

5 Conclusion

The high frequency scattering by impedance double wedge structures using the Extended Spectral Ray Method was studied and uniform diffraction coefficients were presented for up to and including the triple diffraction mechanisms. These were derived in a rigorous manner and include contributions due to surface waves. Indentities given in this paper were crucial to putting the integrands of the diffraction terms in forms amenable to asymptotic evaluation via the modified Pauli-Clemmow method of steepest descents.

The double wedge structures analyzed were divided into two categories. The first included some special geometries in which the adjacent sides of the common wedge face did not intersect. Examples of these structures were the thick impedance half plane and the impedance insert in a full plane. Computations of the diffracted fields were also presented and were found to agree with corresponding data generated via the Angular Spectrum Method (ASM)-Generalized Scattering Matrix Formulation (GSMF) and Moment Method approaches. In particular the thick impedance half plane with a width of 0.01λ compared quite well with ASM-GSMF data.

The second category of double wedge structures included convex polygonal cylinders. In this case, an additional third order mechanism was derived to be used in conjunction with the previous coefficients to characterize the contribution of all triple diffraction mechanisms. The results from impedance cylinders of triangular cross section were further examined in order to examplify the necessity of including higher order mechanisms. The total analytic solution compared quite

well with moment method data for cylinder sides as small as $\frac{\lambda}{4}$.

Finally, for the sake of completeness, the scattering by an impedance strip was presented. The results compared well with moment method data and with an alternate ESRM formulation using Senior's half plane diffraction integral. We noted, however,that the Maliuzhinets wedge diffraction integral employed with ESRM gave the additional freedom of having non-equal impedances on each face of the strip.

References

[1] Tiberio, R., G. Manara, G. Pelosi and R. G. Kouyoumjian , High-Frequency diffraction by a double wedge, IEEE/APS Symposium and National Radio Science Meeting in Vancouver, Canada, June 1985

[2] Rahmat-Samii, Y. and R. Mittra (1977), A spectral domain interpretation of high-frequency diffraction phenomena, *IEEE Trans. Antennas Propag.*, AP-25, 676-687

[3] Volakis, J. L. (1987), Scattering by a thick impedance half plane, *Radio Sci.*, in press

[4] Volakis, J. L. and M. A. Ricoy (1987), Diffraction by a thick perfectly conducting half plane, *IEEE Trans. Antennas Propag.*, January

[5] Senior, T.B.A. (1952), Diffraction by a semi-infinite metallic sheet, *Proc. Roy. Soc.* (London), A 213(1115), 436-458

[6] Maliuzhinets, G. D. (1958), Excitation, reflection and emission of surface waves from a wedge with given face impedances, *Sov. Phys. Dokl.*, Engl. Transl., 3, 752-755

[7] Herman M. I., J. L. Volakis and T. B. A. Senior, Analytic expressions for a function occurring in diffraction theory, submitted to *IEEE Trans. Antennas Propag.*

[8] Volakis, J. L. and M. I. Herman (1986), A uniform asymptotic evaluation of integrals, *Proc. IEEE*, Vol. 74, No. 7, 1043-1044

[9] Herman M. I. and J. L. Volakis, High frequency scattering by a resistive strip, submitted to *Radio Sci.*

[10] Kouyoumjian, R.G., and P.H. Pathak (1974), A uniform geometrical theory of diffraction for an edge in a perfectly conducting surface, *Proc. IEEE*, 62(11), 1448-1461

[11] Clemmow,P.C. (1966), The Plane Wave Spectrum Representation of Electromagnetic Fields, Pergamon, New York

[12] Volakis, J. L. and T.B.A. Senior (1985), Simple expressions for a function occurring in diffraction theory, *IEEE Trans. Antennas Propag.*,AP-33, 678-680

[13] Tiberio, R. and G. Pelosi (1983), High frequency scattering from the edges of impedance discontinuites on a flat plane, *IEEE Trans. Antennas Propag.*, AP-31, 590-596

[14] Wang, N. (1976), Self-consistent GTD formulation for conducting cylinders with arbitrary convex cross section, *IEEE Trans. Antennas Propag.*, AP-24, 463-468

[15] Herman, M. I., personal notes

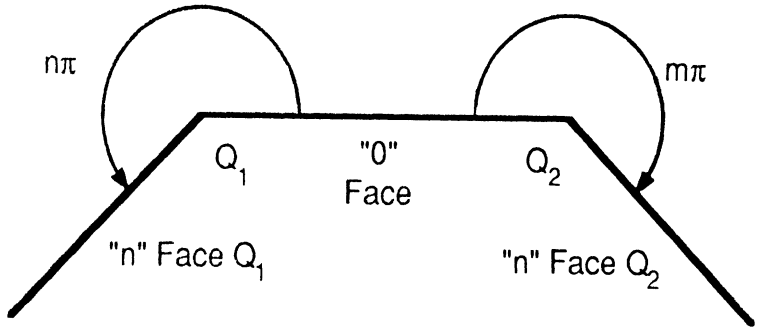

Fig. 1. Isolated impedance double wedge structure.

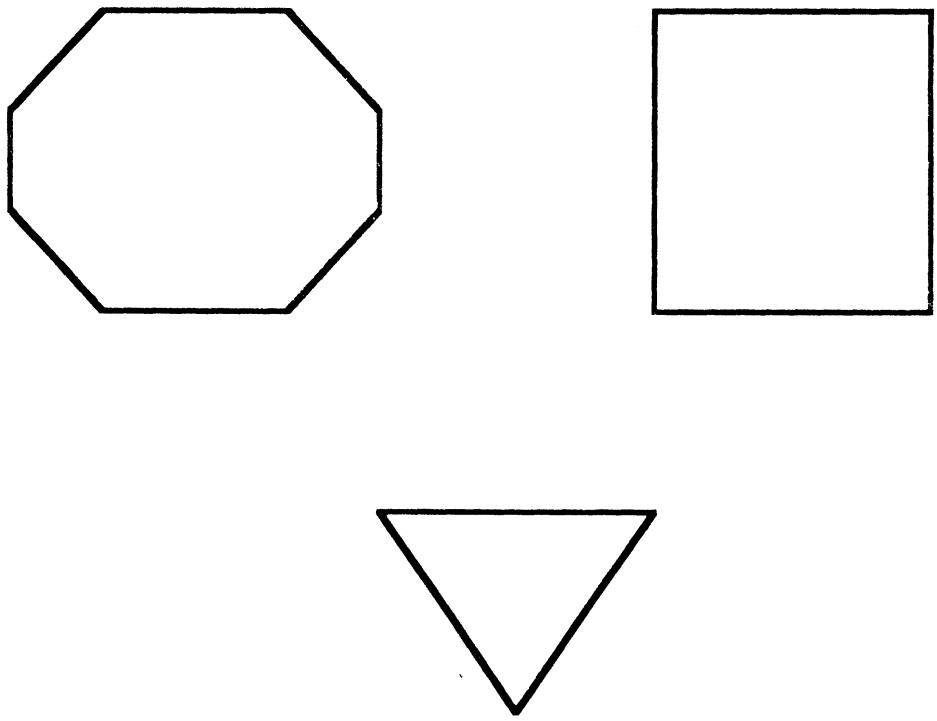

Fig. 2. Examples of convex cylindrical polygons.

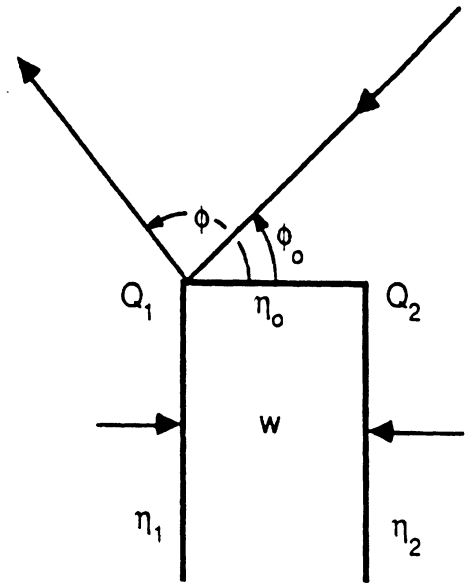

Fig. 3. Thick impedance half plane.

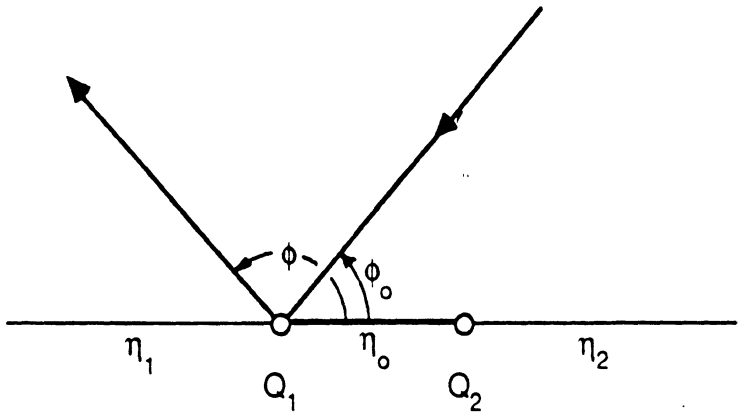

Fig. 4. Impedance insert in a full plane.

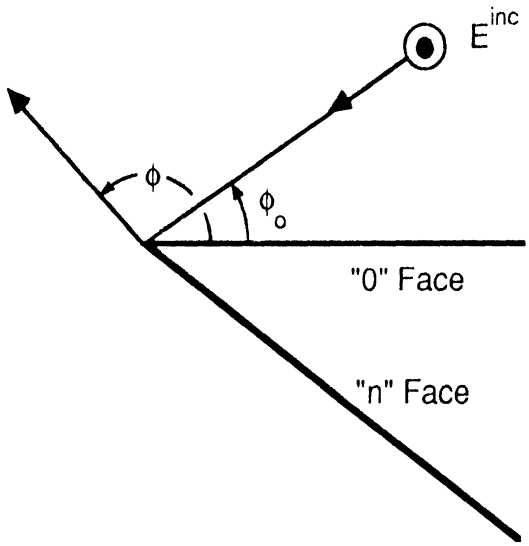

Fig. 5. Isolated wedge.

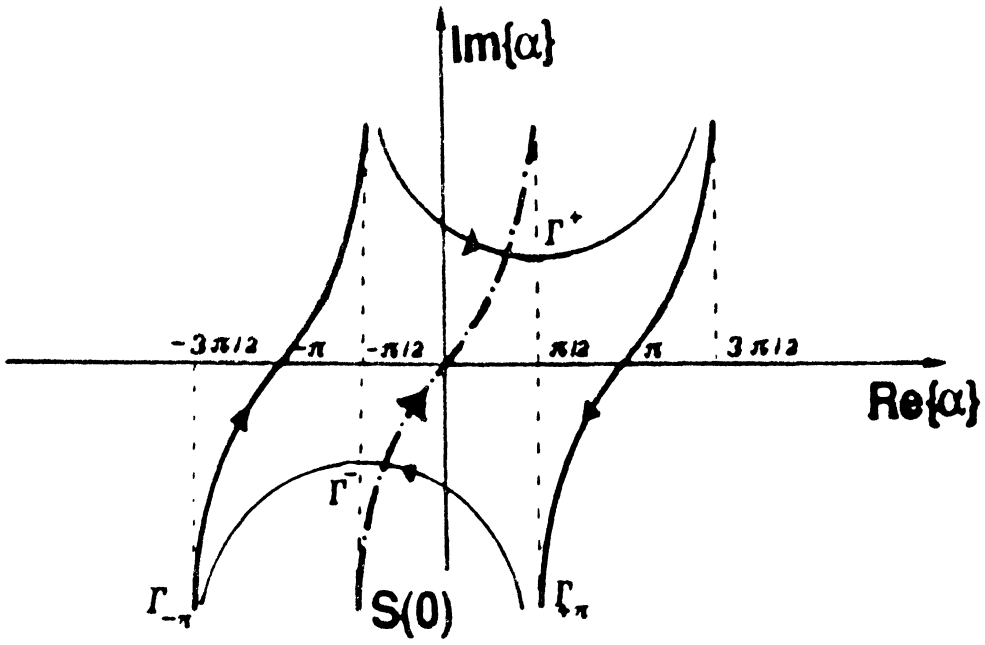

$$C = \Gamma^{-} + \Gamma^{+}$$

Fig. 6. Topology for the integral representation of the diffracted field. [13]

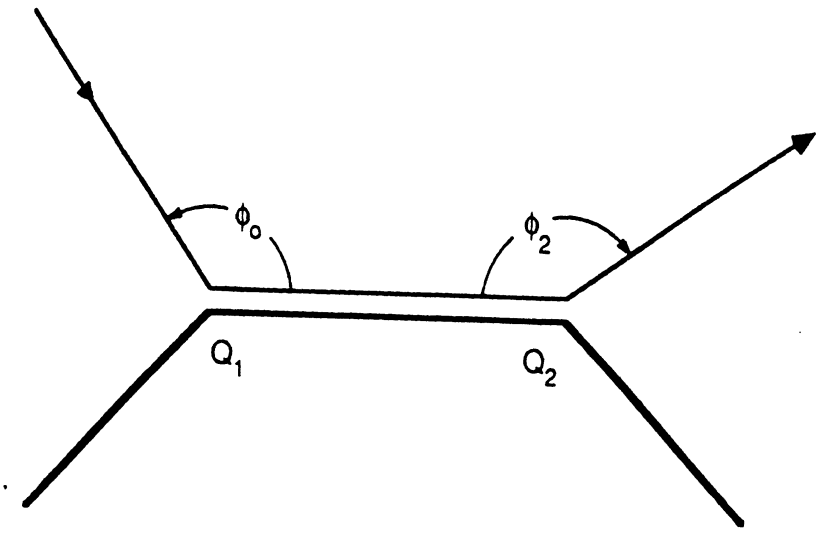

Fig. 7. Second order diffraction mechanism.

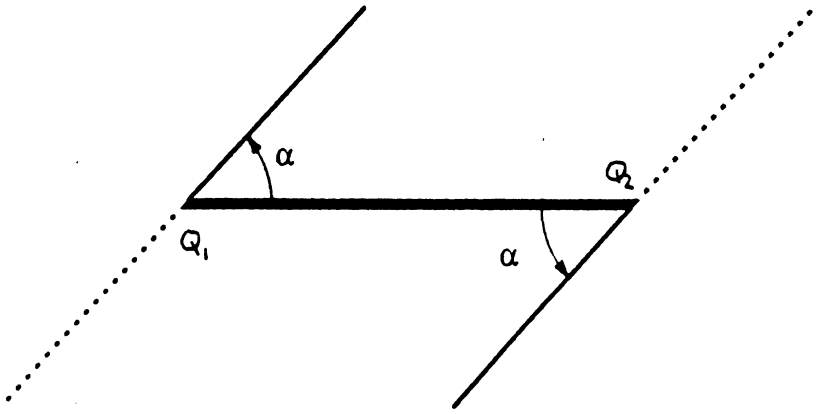

Fig. 8. Spectral plane wave with angle $-\alpha$ at Q_1 has an angle α at Q_2.

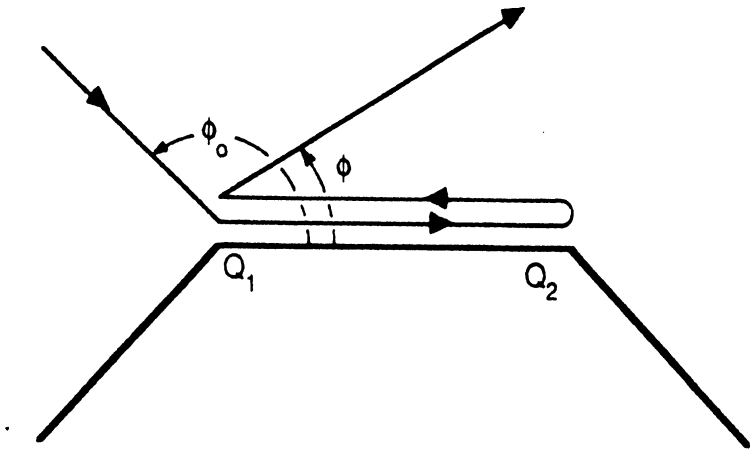

Fig. 9. Triple order diffraction mechanism at Q_1.

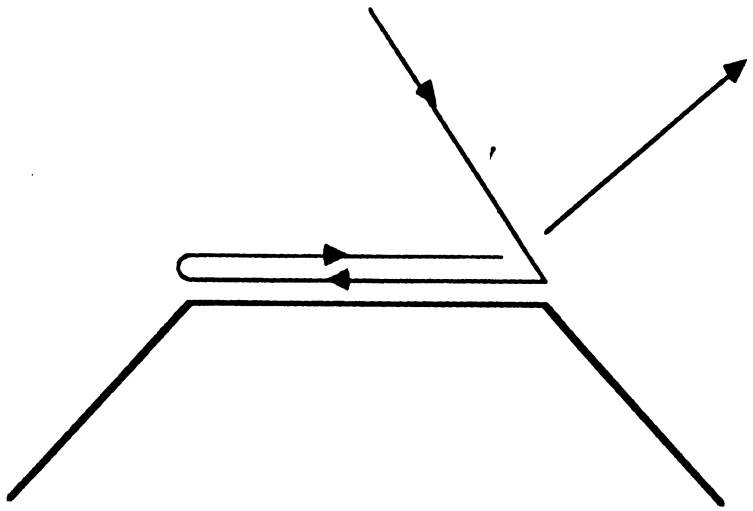

Fig. 10. Triple order diffraction mechanism at Q_2.

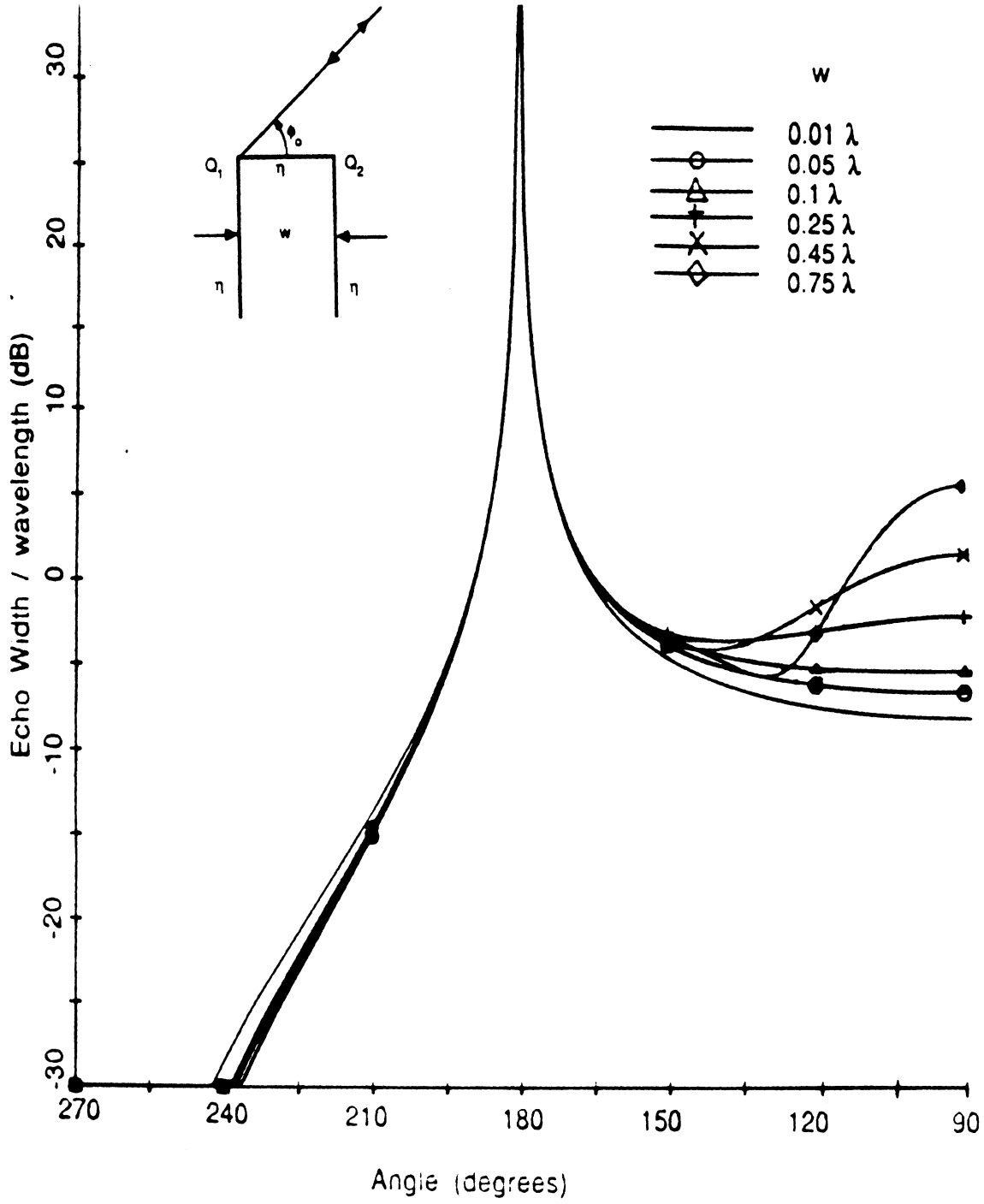

11 (a)

Fig. 11. Backscatter from a perfectly conducting thick half plane (a)E-polarization, (b) H-polarization.
Half plane widths are 0.01λ, 0.05λ, 0.1λ, 0.25λ, 0.45λ, 0.75λ and 0.95λ.

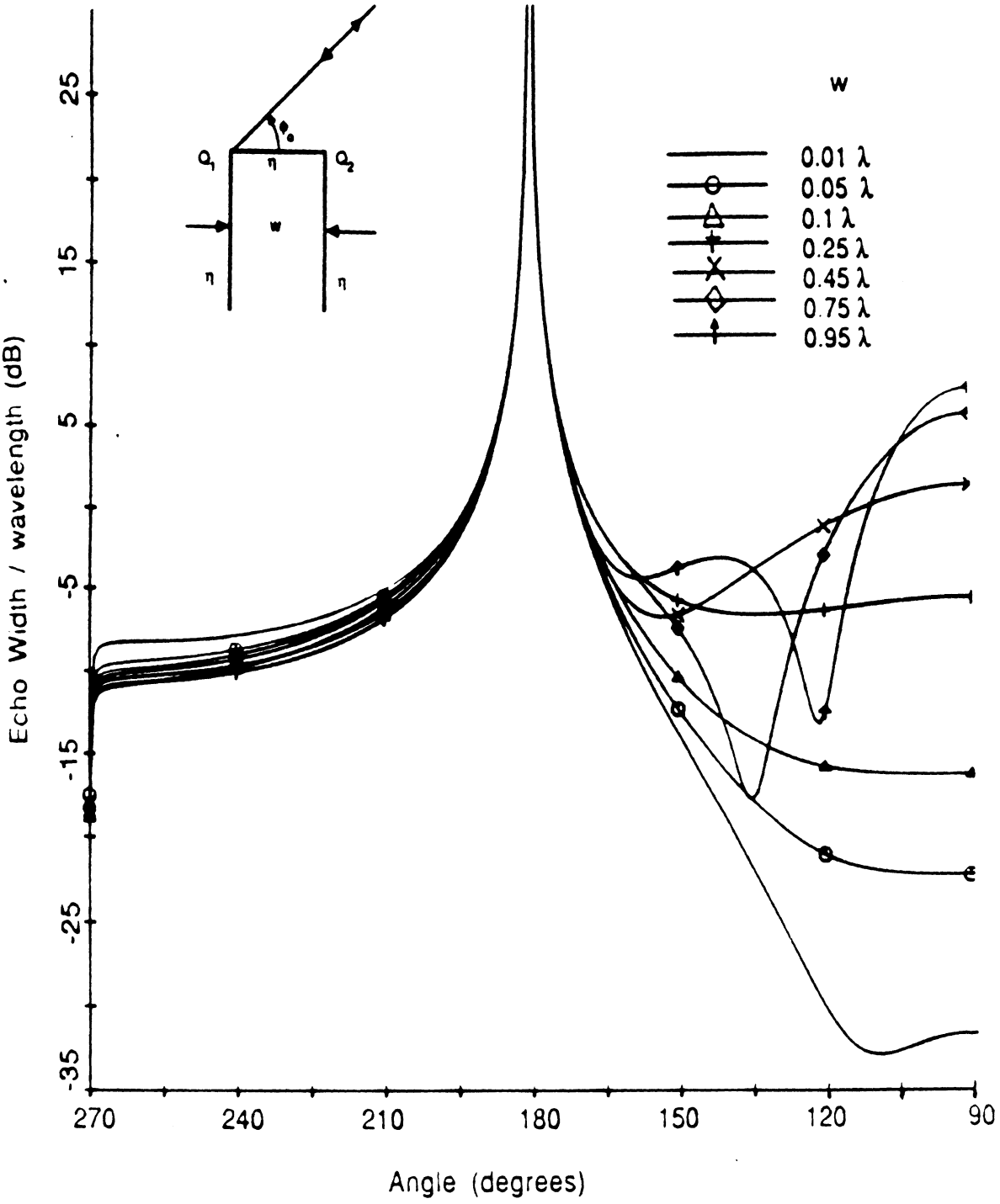
w
0.01 λ
0.05 λ
0.1 λ
0.25 λ
0.45 λ
0.75 λ
0.95 λ
Echo Width / wavelength (dB)
25
15
5
-5
-15
-25
-35
270
240
210
180
150
120
90
Angle (degrees)

11 (b)

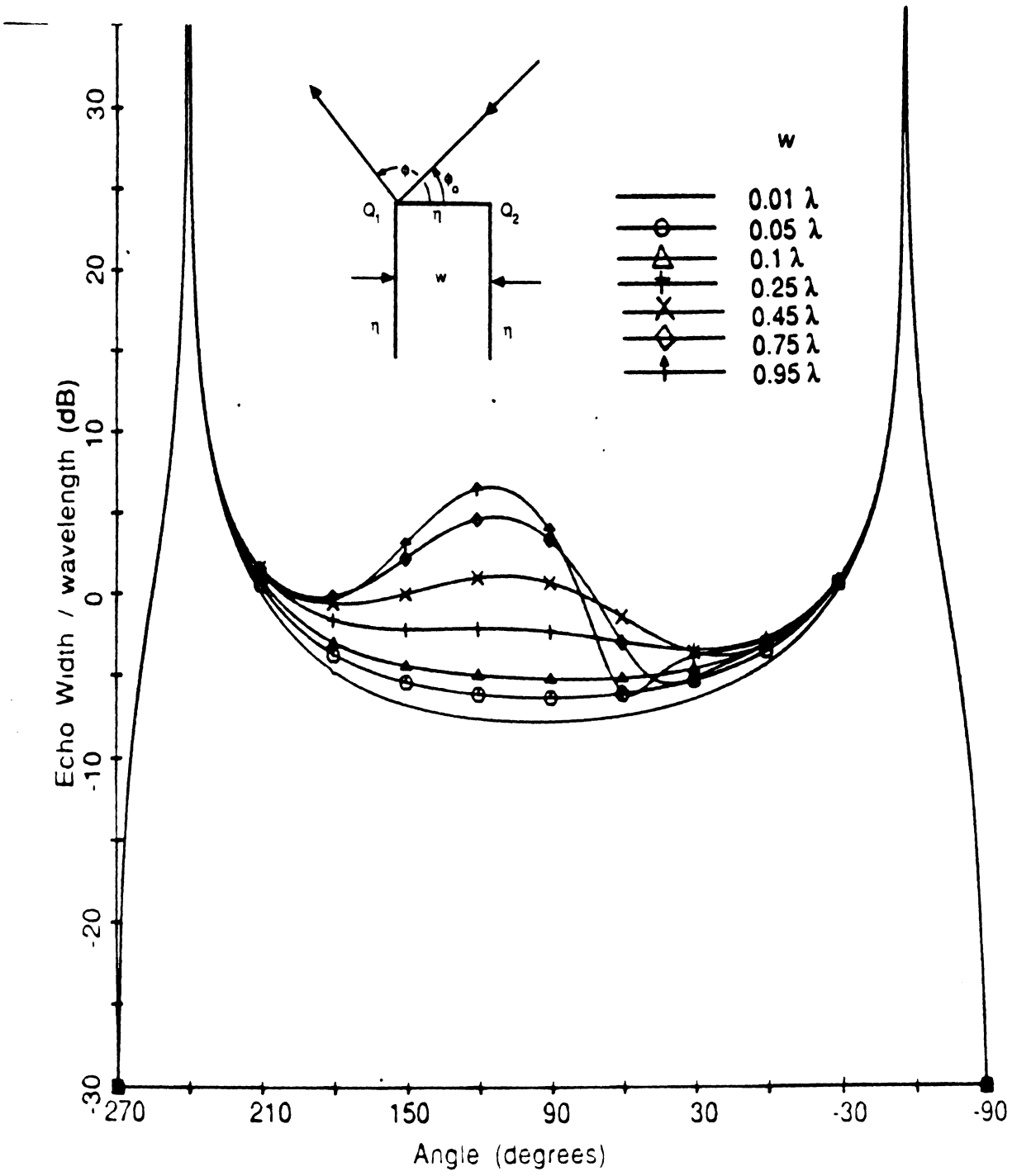

12 (a)

Fig. 12. Bistatic pattern from a perfectly conducting thick half plane (a)E-polarization, (b)H-polarization, with an angle of incidence of $\phi_o = 60°$. Half plane widths are 0.01λ, 0.05λ, 0.1λ, 0.25λ, 0.45λ, 0.75λ and 0.95λ.

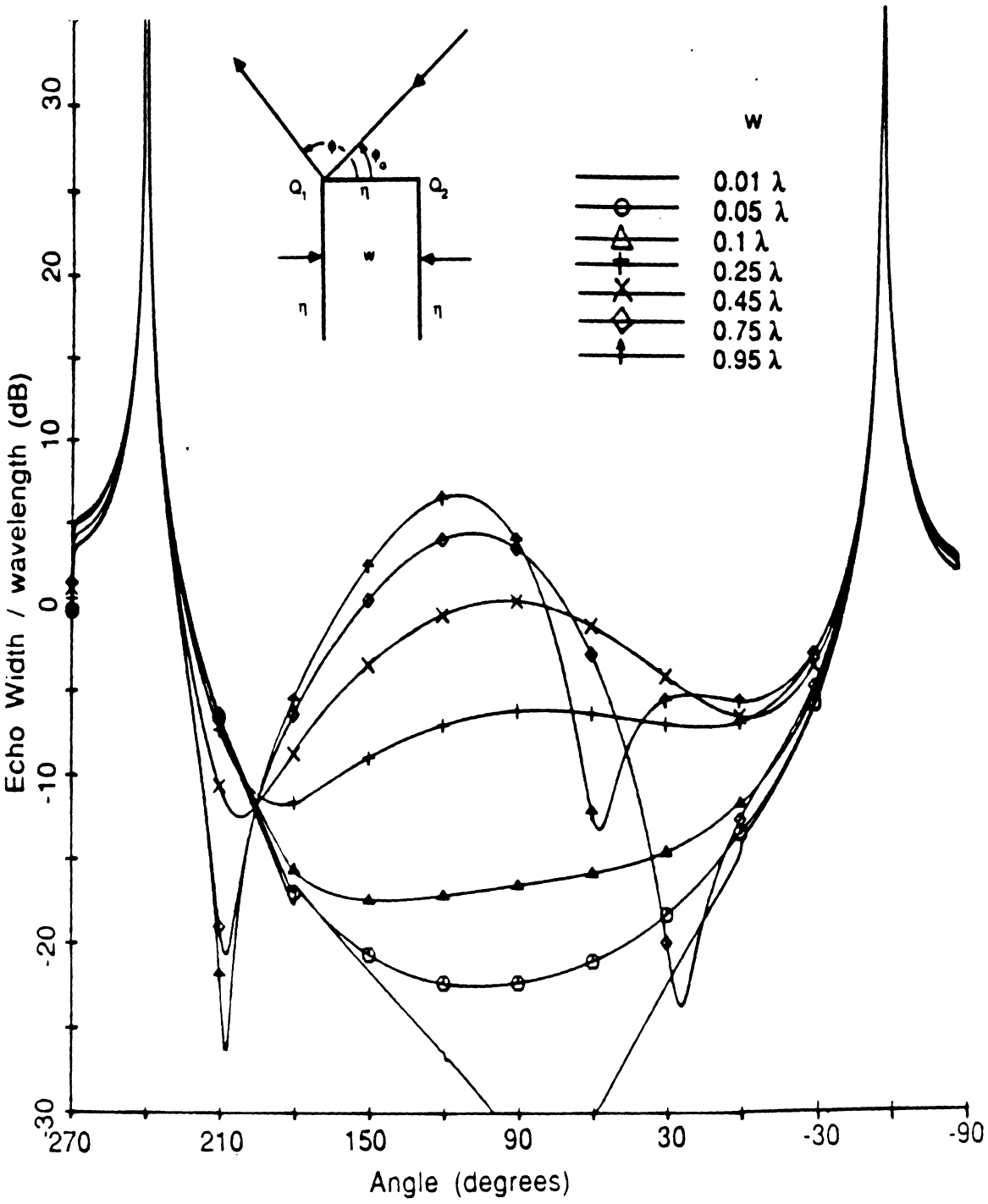
w
0.01 λ
0.05 λ
0.1 λ
0.25 λ
0.45 λ
0.75 λ
0.95 λ
Echo Width / wavelength (dB)
30
20
10
0
-10
-20
-30
270
210
150
90
30
-30
-90
Angle (degrees)

12 (b)

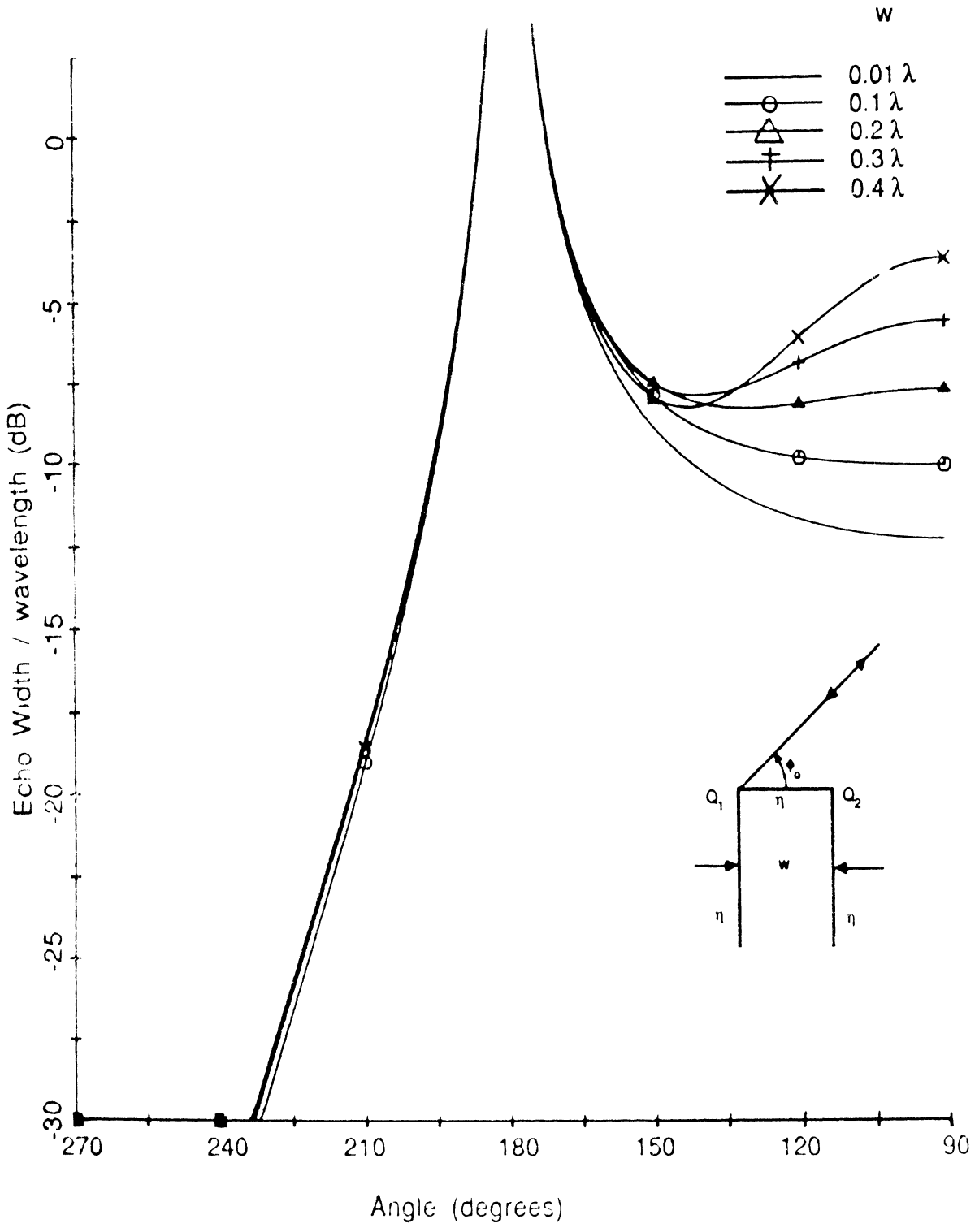

13 (a)

Fig. 13. Backscatter from a thick impedance half plane, E-polarization with normalized impedance (a) $\eta = 0.25$, (b)$\eta = 4$, (c)$\eta = 2 + j2$, and (d) $\eta = 2 - j2$. Half plane widths are 0.01λ, 0.1λ, 0.2λ, 0.3λ and 0.4λ .

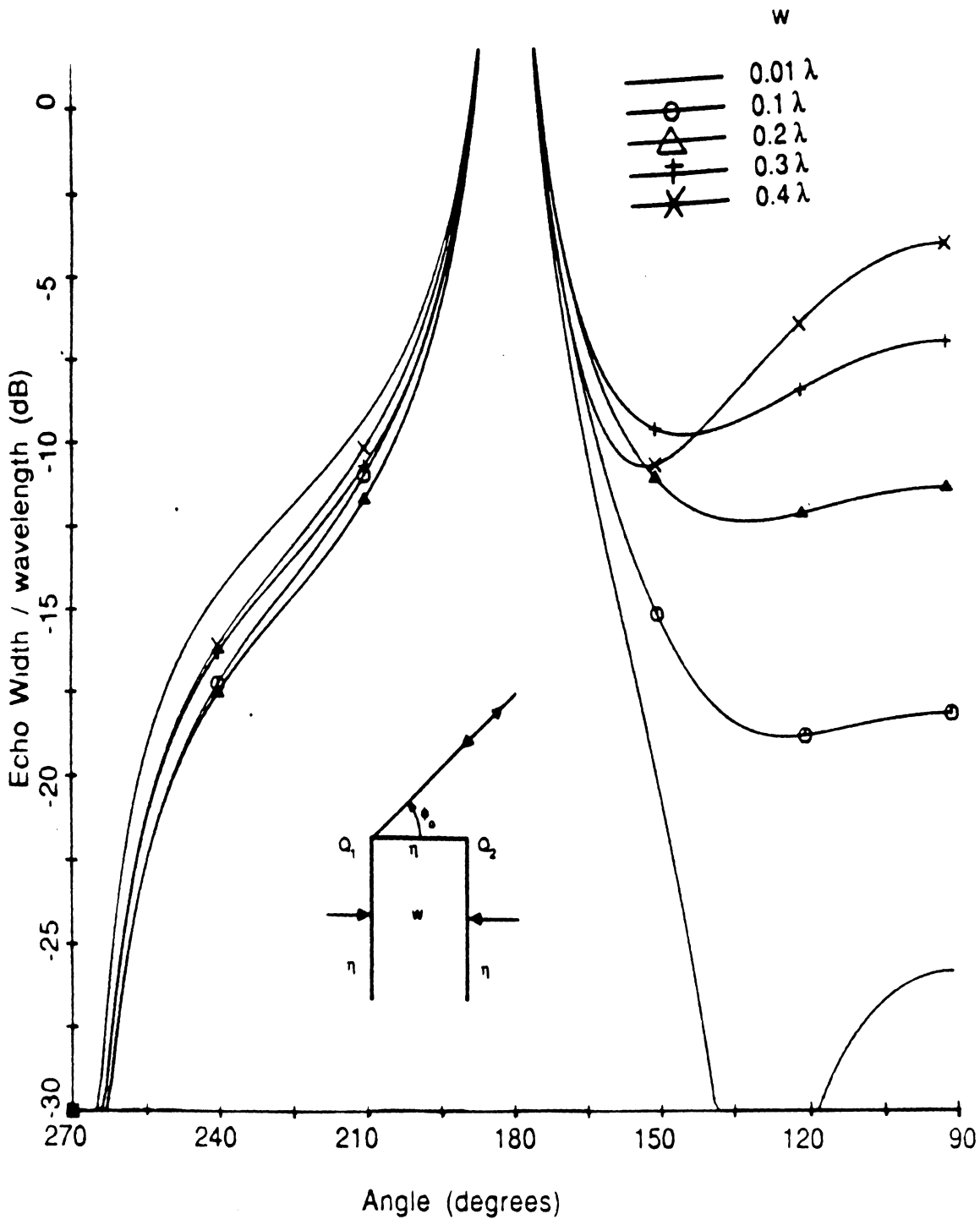
w
0.01 λ
0.1 λ
0.2 λ
0.3 λ
0.4 λ
Echo Width / wavelength (dB)
0
-5
-10
-15
-20
-25
-30
270
240
210
180
150
120
90
Angle (degrees)
ϕ_0
Q_1
Q_2
η
w
η
η

13 (b)

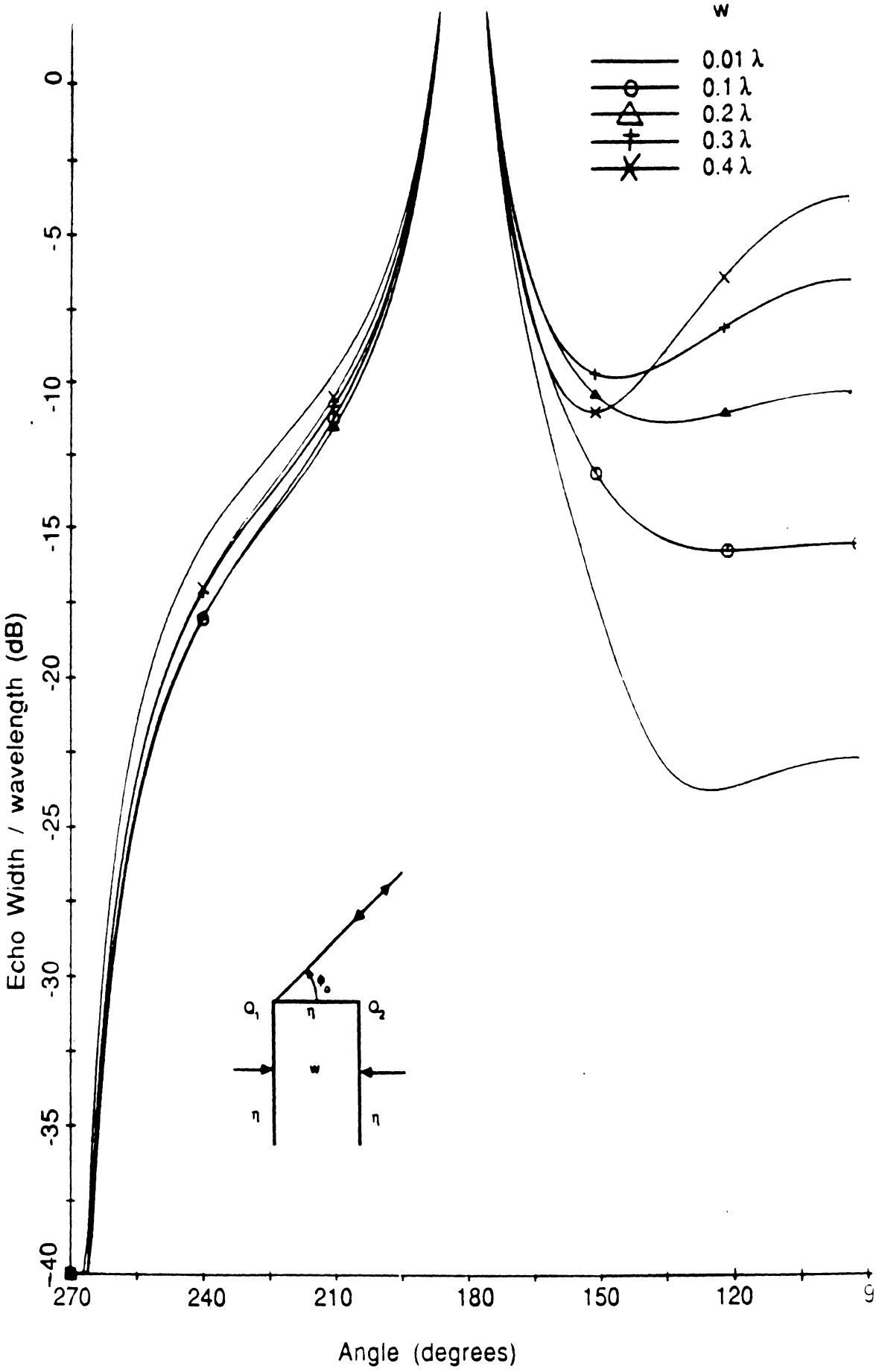
w
0.01 λ
0.1 λ
0.2 λ
0.3 λ
0.4 λ
Echo Width / wavelength (dB)
0
-5
-10
-15
-20
-25
-30
-35
-40
270
240
210
180
150
120
Angle (degrees)
θ_0
θ_1
θ_2
w

13 (c)

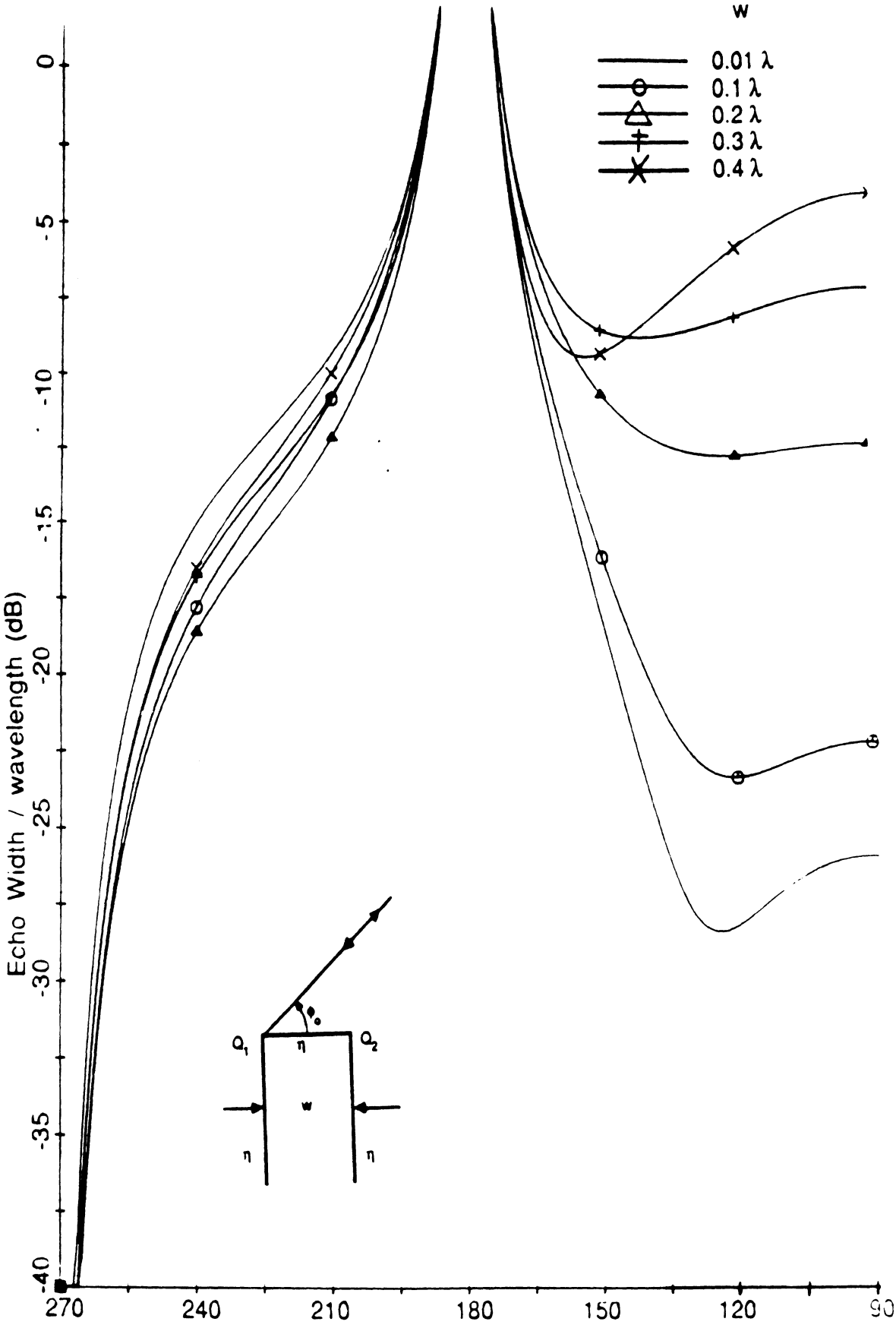
w
0.01 λ
0.1 λ
0.2 λ
0.3 λ
0.4 λ
Echo Width / wavelength (dB)
0
-5
-10
-15
-20
-25
-30
-35
-40
270
240
210
180
150
120
90
Angle (degrees)
ρ_1
ρ_2
η
w
η
η

13 (d)

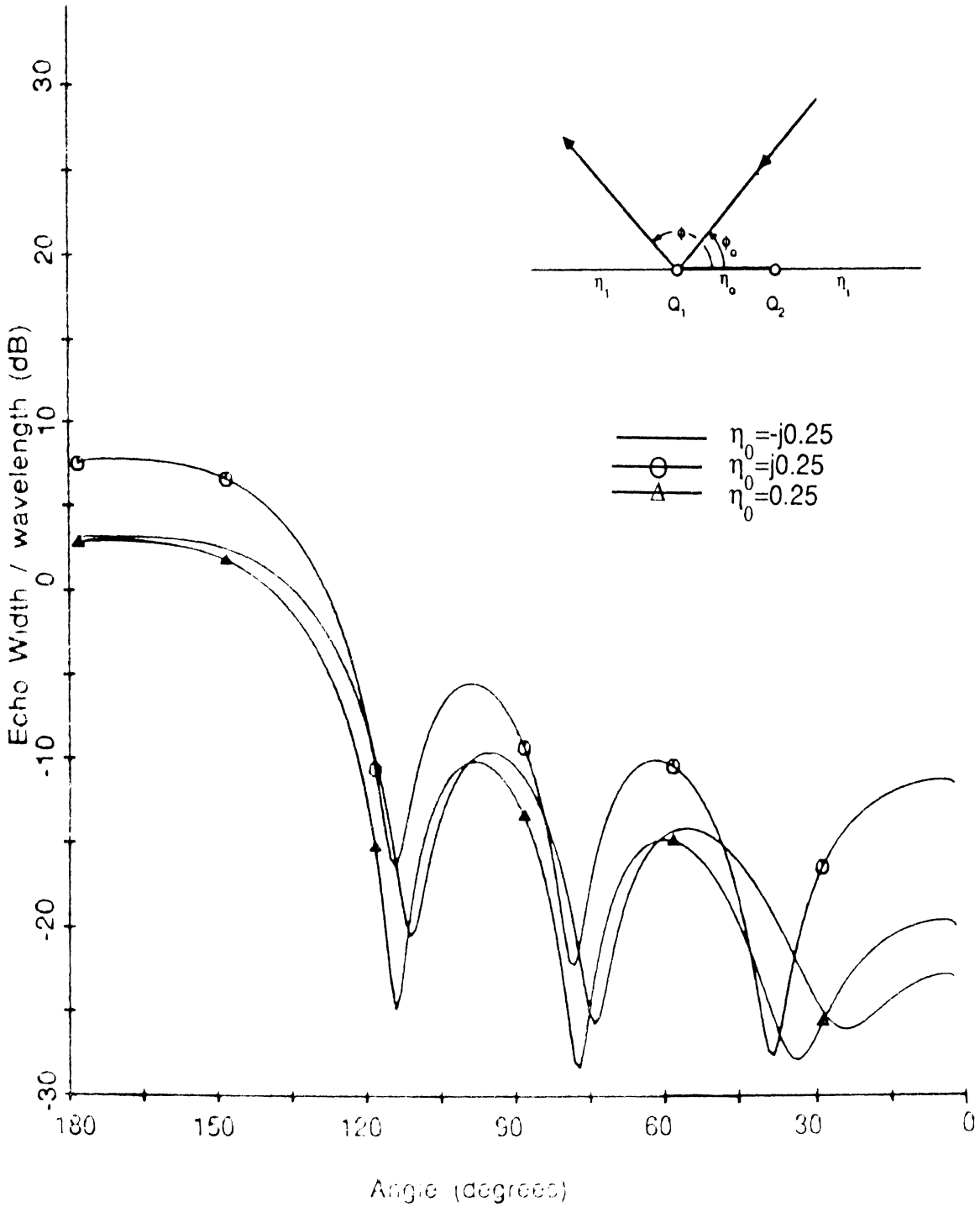

Fig. 14. Bistatic pattern from an impedance insert, H-polarization with an angle of incidence $\phi_0 = 1°$. The insert impedances are $\eta_o = -j0.25$, $\eta_o = j0.25$ and $\eta_o = .25$. The outer impedance is $\eta_1 = 0$ and the width of the strip is 1.6λ.

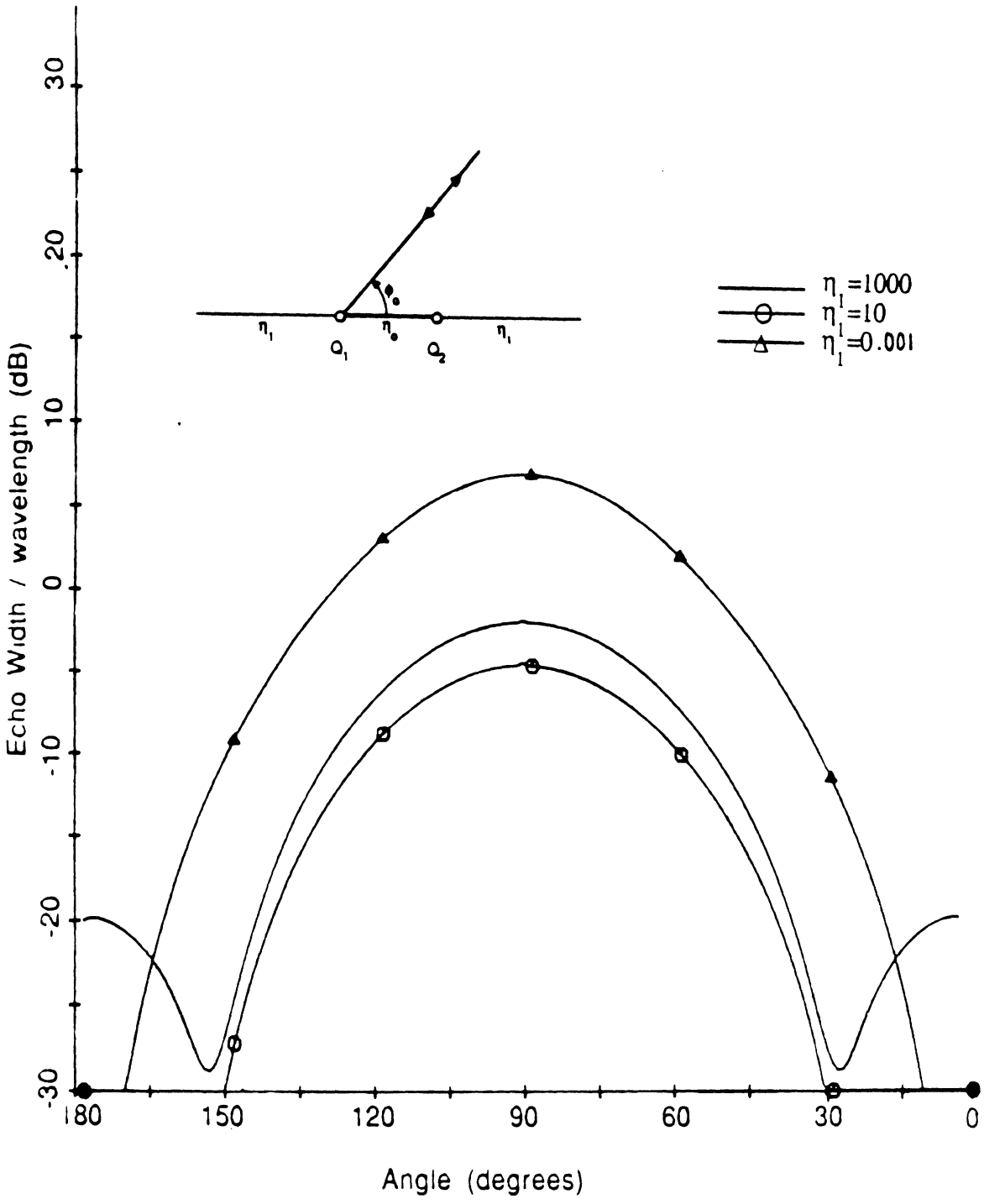

15 (a)

Fig. 15. Backscatter from an impedance insert, E-polarization.
The insert impedance is held constant at $\eta_o = 2 - j1$.
The outer impedances are $\eta_1 = 1000$, $\eta_1 = 10$ and $\eta_1 = 0.001$.
Strip width is (a) 0.5λ and (b) 1λ.

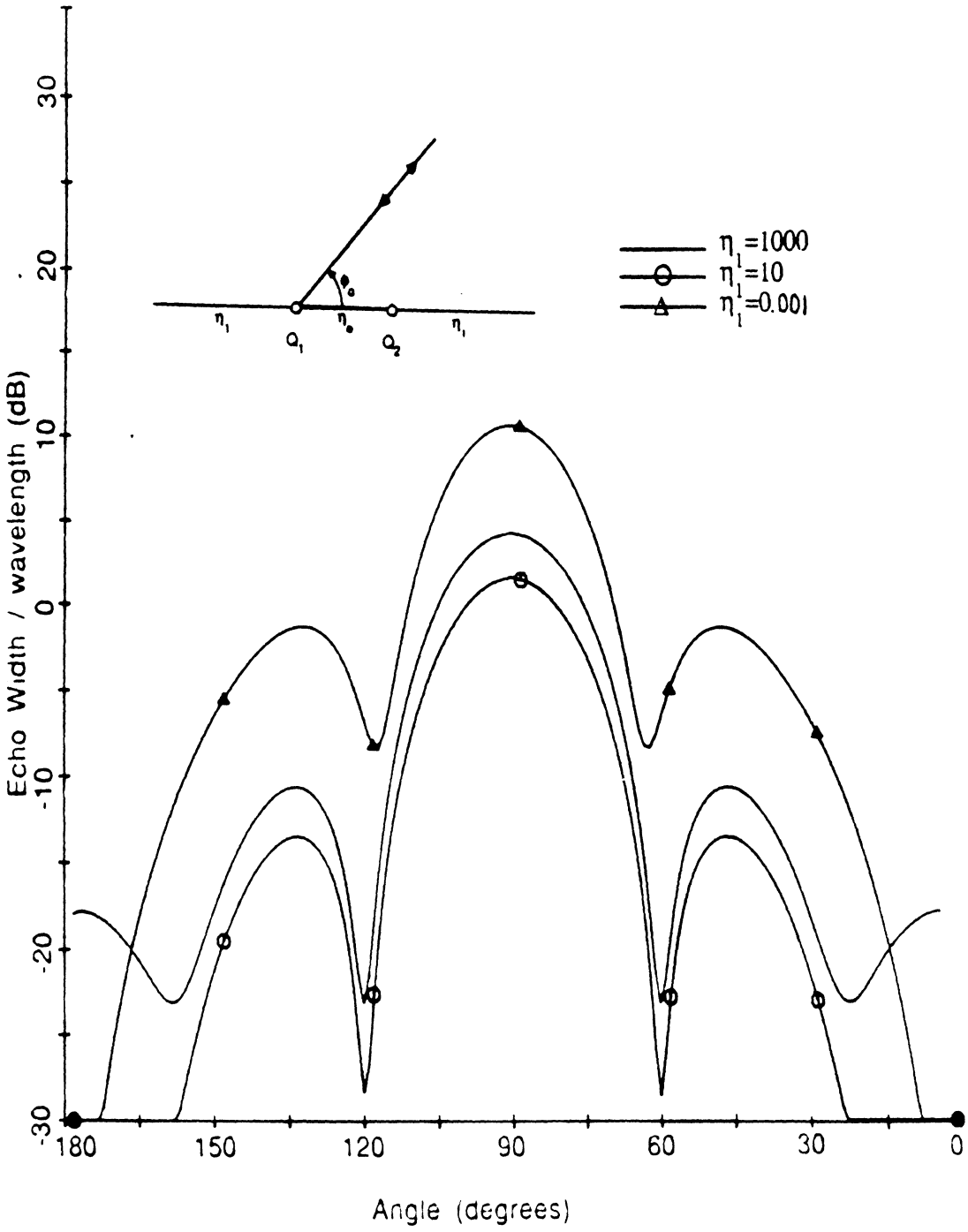
30
20
10
0
-10
-20
-30
Echo Width / wavelength (dB)
180
150
120
90
60
30
0
Angle (degrees)
η_1=1000
η_1=10
η_1=0.001
η_1
η_0
Q_1
Q_2
η_1

15 (b)

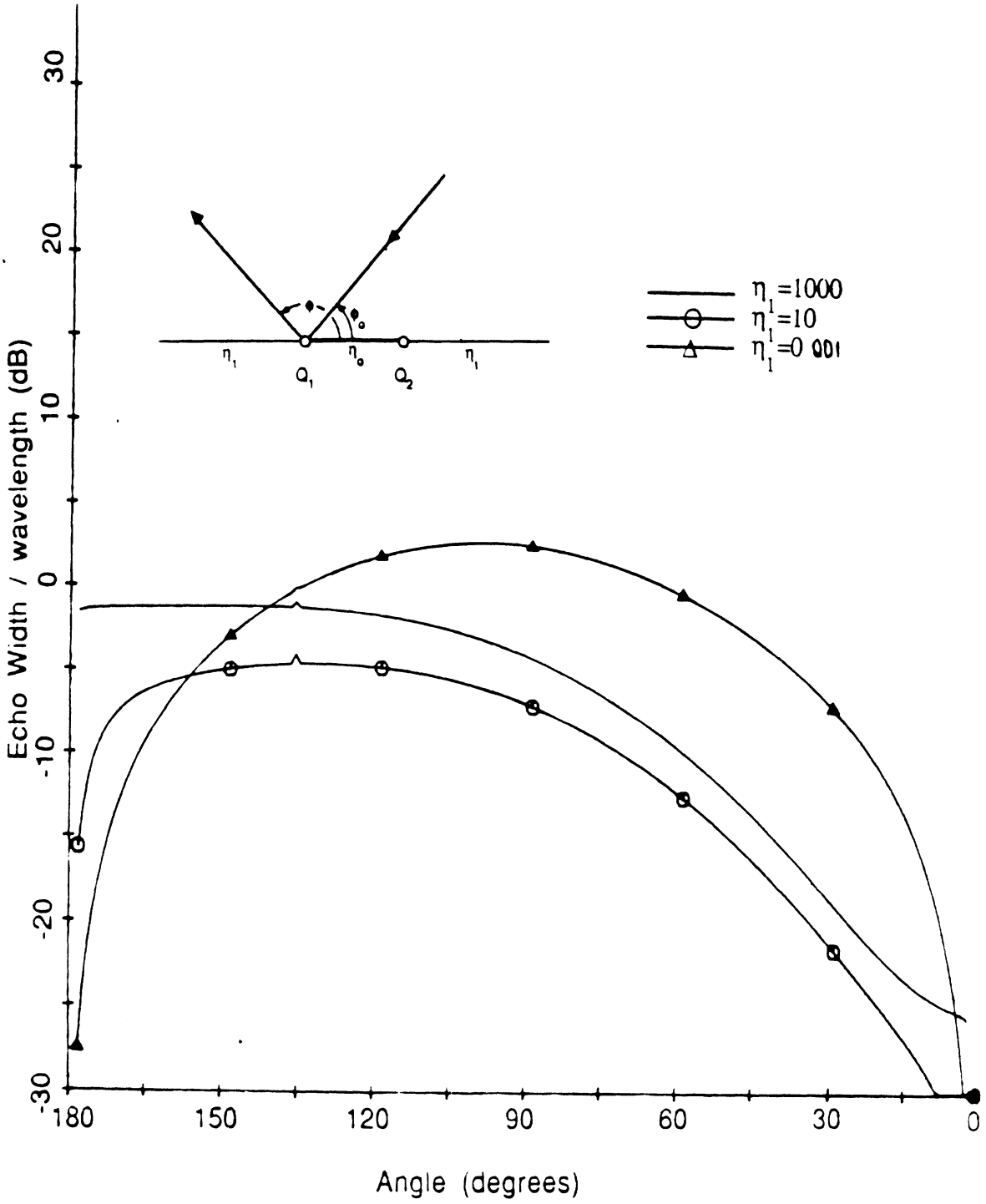

16 (a)

Fig. 16. Bistatic pattern from an impedance insert, E-polarization with an angle of incidence $\phi_o = 45°$.
The insert impedance is held constant at $\eta_o = 2 - j1$.
The outer impedances are $\eta_1 = 1000$, $\eta_1 = 10$ and $\eta_1 = 0.001$.
Strip width is (a) 0.5λ and (b) 1λ.

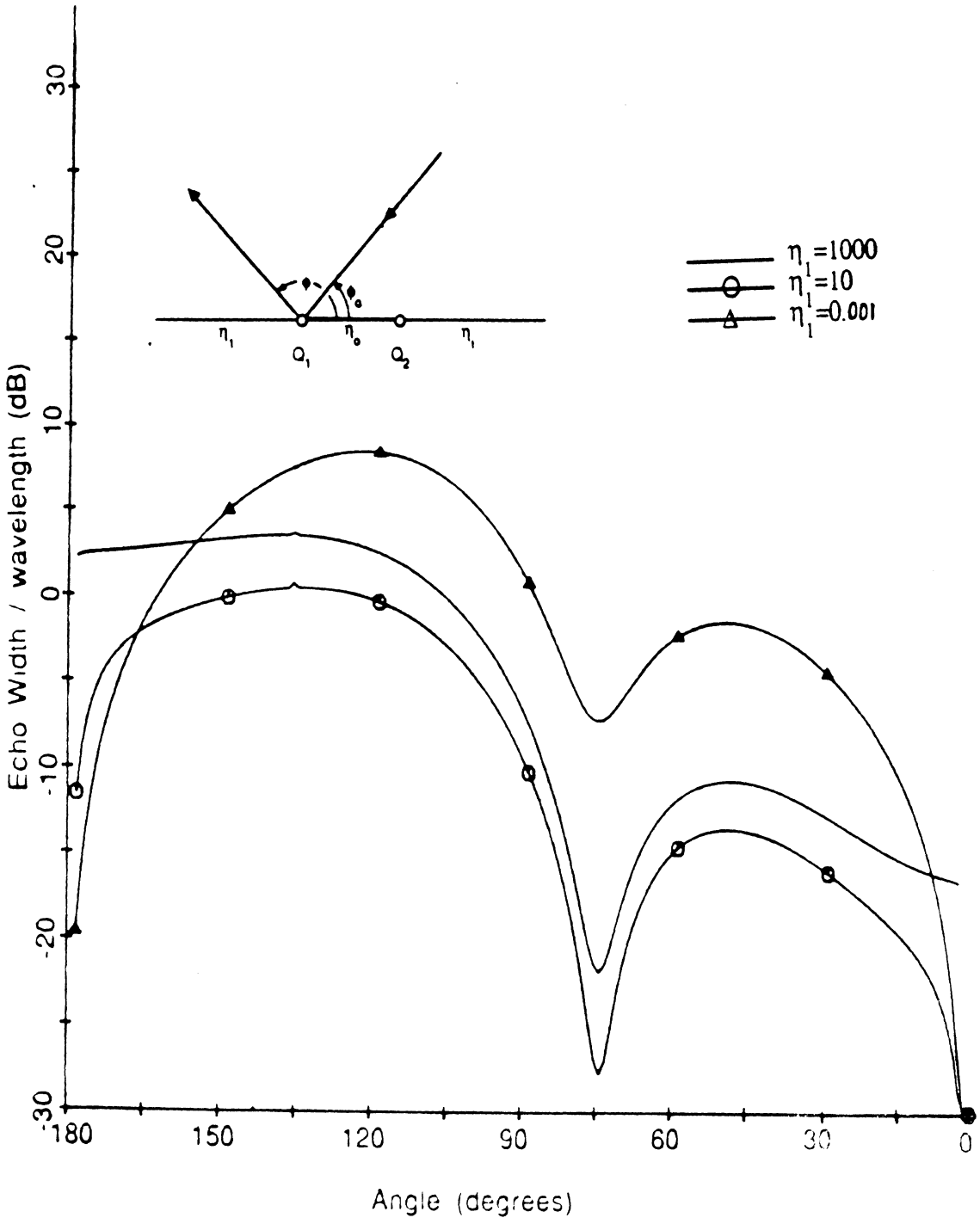
30
20
10
0
-10
-20
-30
Echo Width / wavelength (dB)
180
150
120
90
60
30
0
Angle (degrees)
η_1=1000
η_1=10
η_1=0.001
η_1
η_0
η_1
Q_1
Q_2

16 (b)

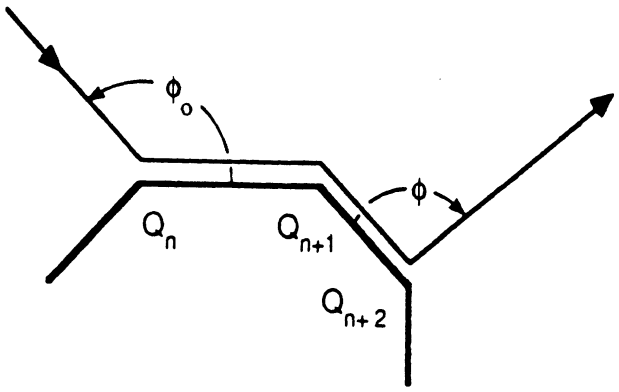

Fig. 17. Triple diffraction mechanism involving three vertices.

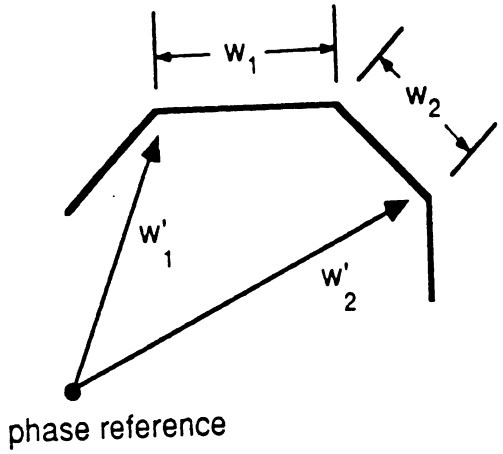

Fig. 18. Geometry of triple diffraction mechanism involving three vertices.

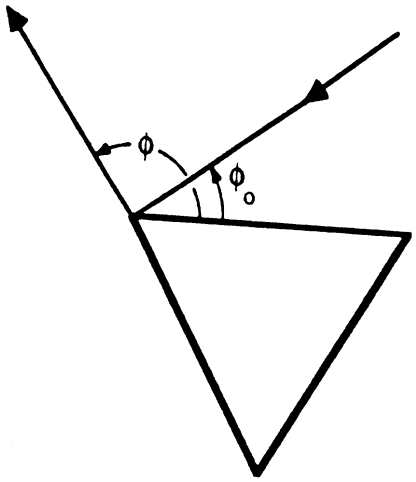

(a)

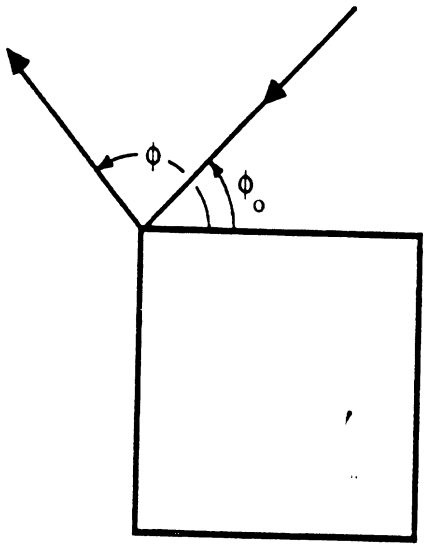

(b)

Fig. 19. (a) Equilateral triangular and (b) square cylinders.

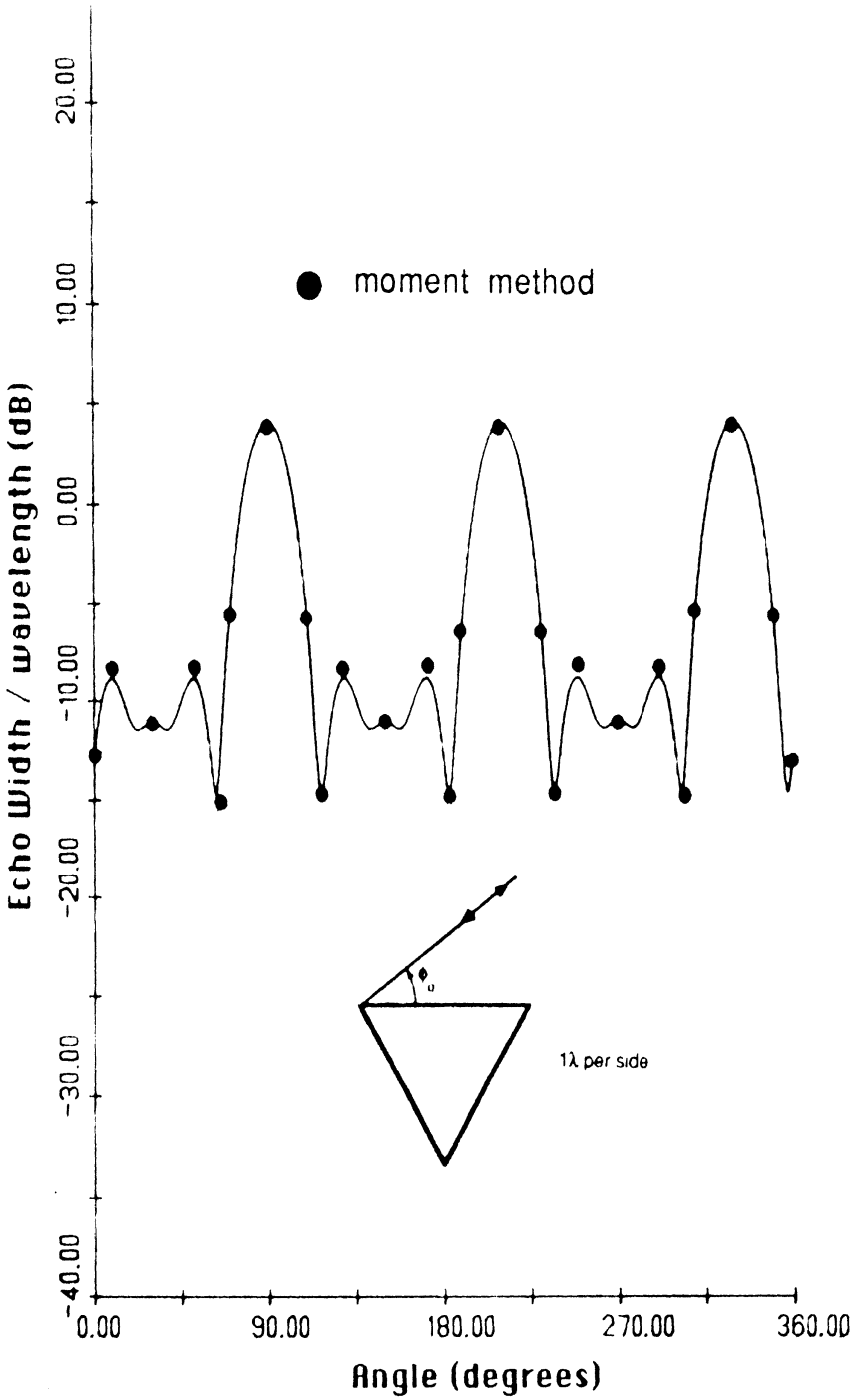

20 (a)

Fig. 20. Comparison of backscatter from an equilateral triangular impedance cylinder, E-polarization, with moment method results. The impedance on all faces are (a) $\eta = 2 + j2$, 1λ in length, (b) $\eta = 2 - j2$, 1λ in length, (c) $\eta = 2 + j2$, 0.5λ in length, (d) $\eta = 2 - j2$, 0.5λ in length, (e) $\eta = 2 + j2$, 0.25λ in length, (f) $\eta = 2 - j2$, 0.25λ in length.

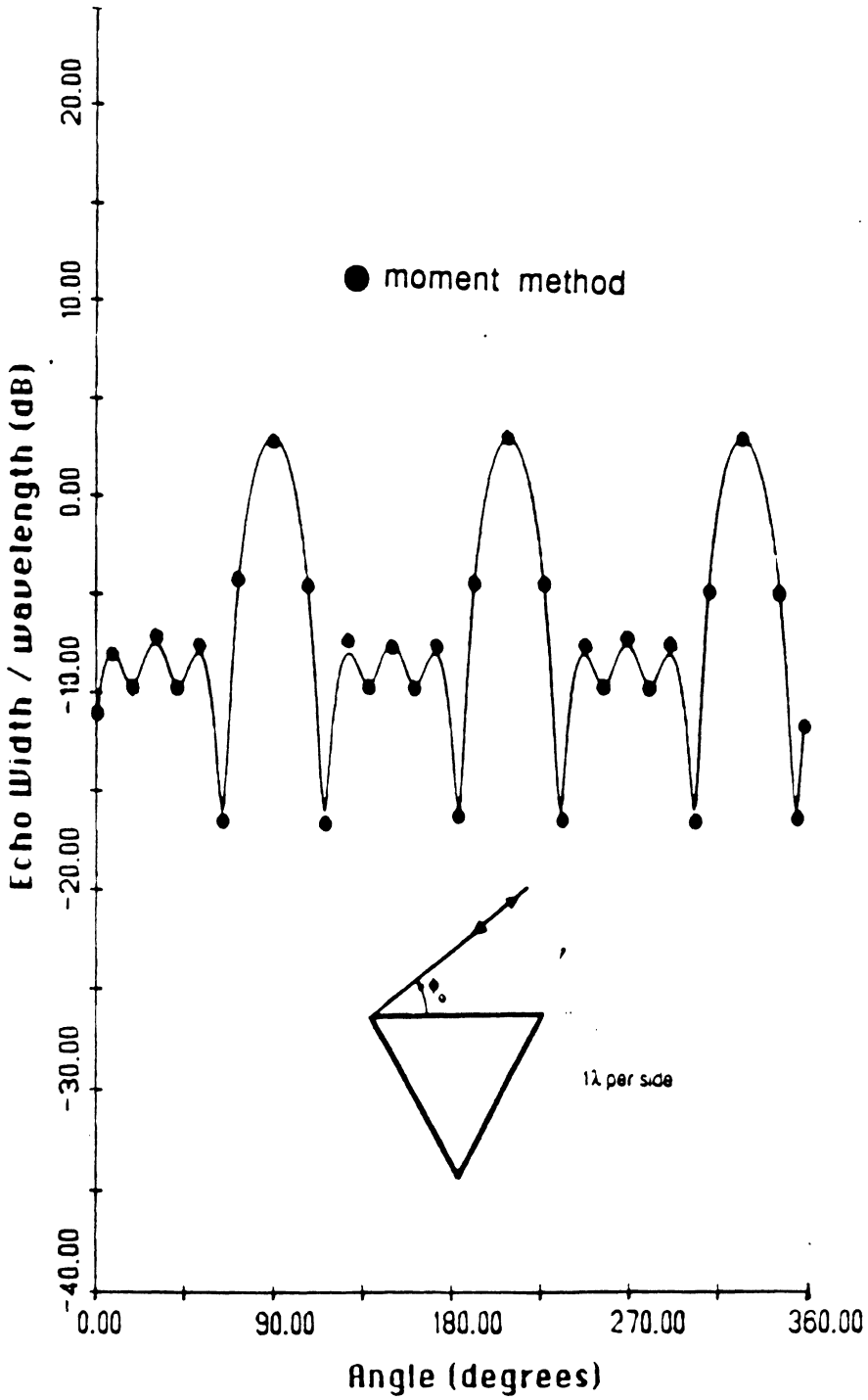
moment method
Echo Width / wavelength (dB)
20.00
10.00
0.00
-10.00
-20.00
-30.00
-40.00
0.00
90.00
180.00
270.00
360.00
Angle (degrees)
1λ per side

20 (b)

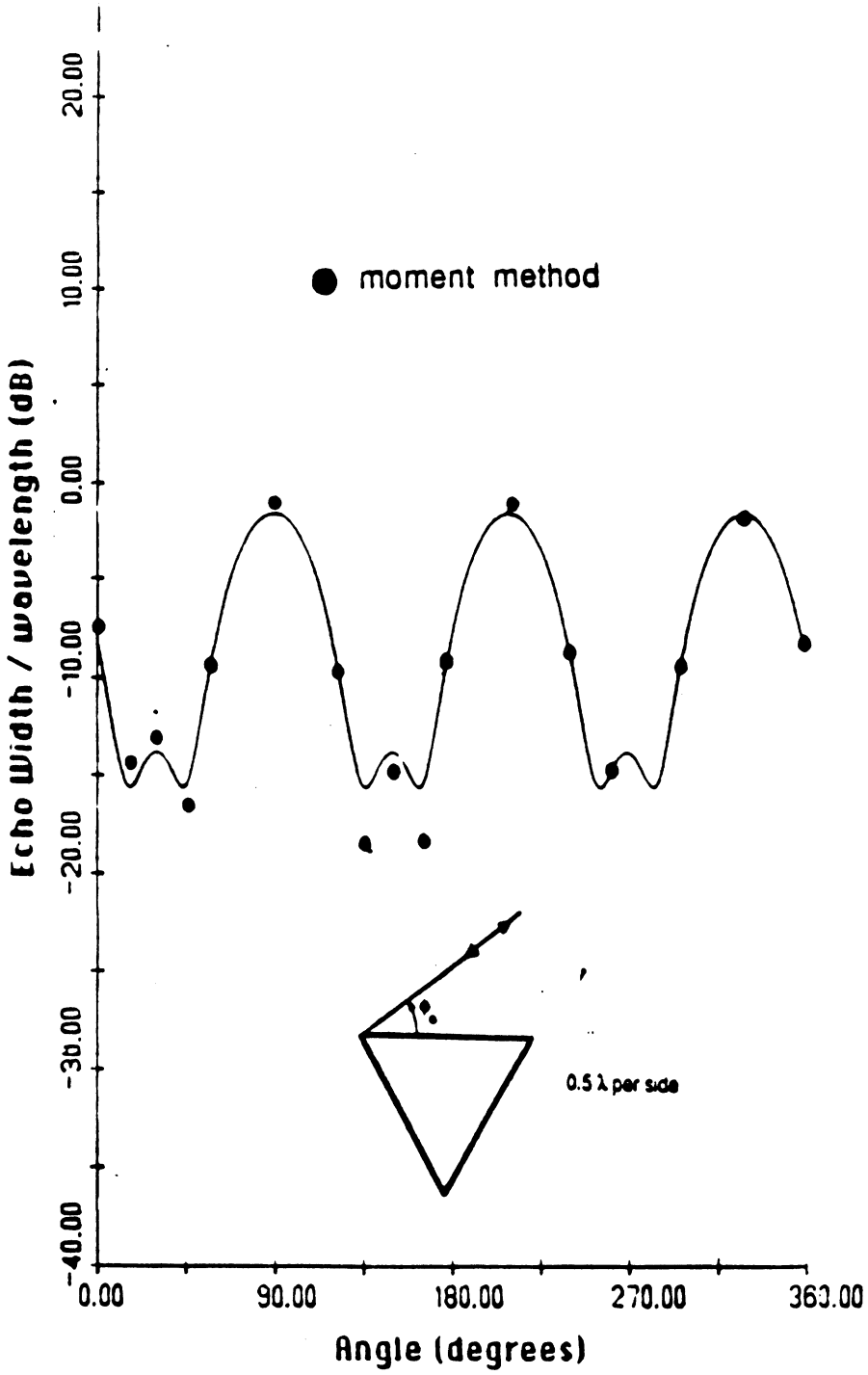
moment method
Echo Width / wavelength (dB)
20.00
10.00
0.00
-10.00
-20.00
-30.00
-40.00
0.00
90.00
180.00
270.00
360.00
Angle (degrees)
0.5 λ per side

20 (c)

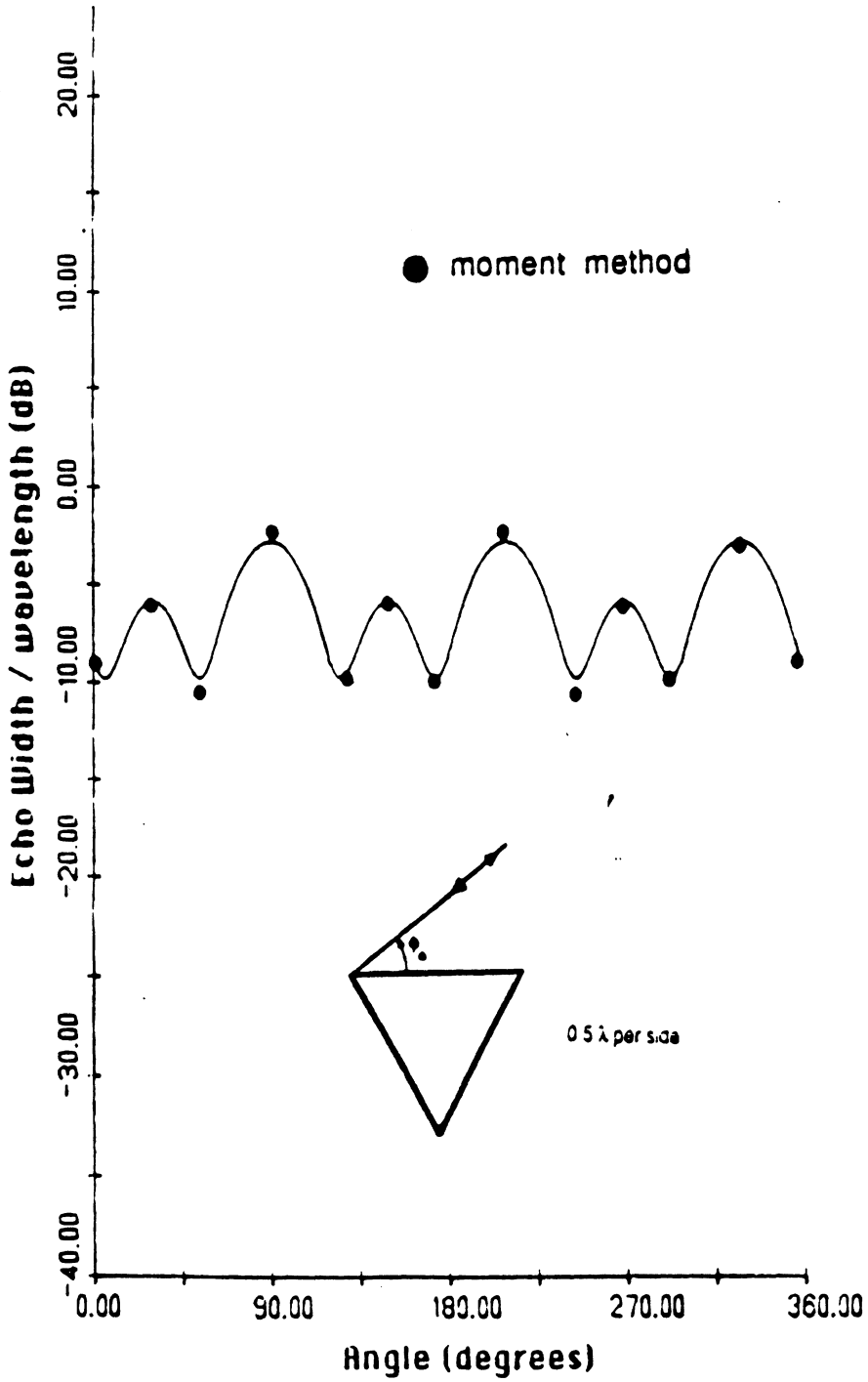
moment method
Echo Width / wavelength (dB)
20.00
10.00
0.00
-10.00
-20.00
-30.00
-40.00
0.00
90.00
180.00
270.00
360.00
Angle (degrees)
0.5 λ per side

20 (d)

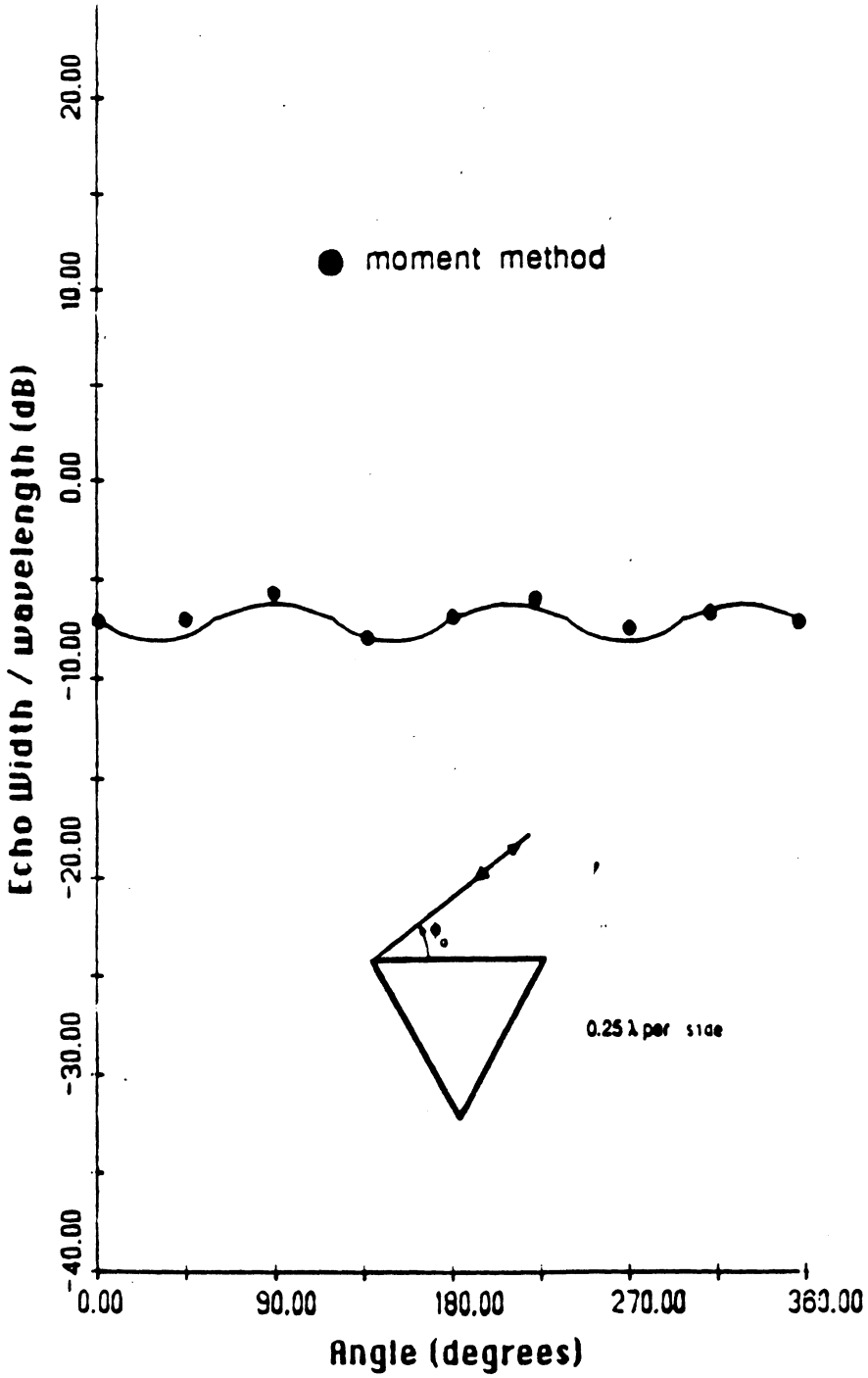
moment method
Echo Width / wavelength (dB)
20.00
10.00
0.00
-10.00
-20.00
-30.00
-40.00
0.00
90.00
180.00
270.00
360.00
Angle (degrees)
0.25 λ per side

20 (e)

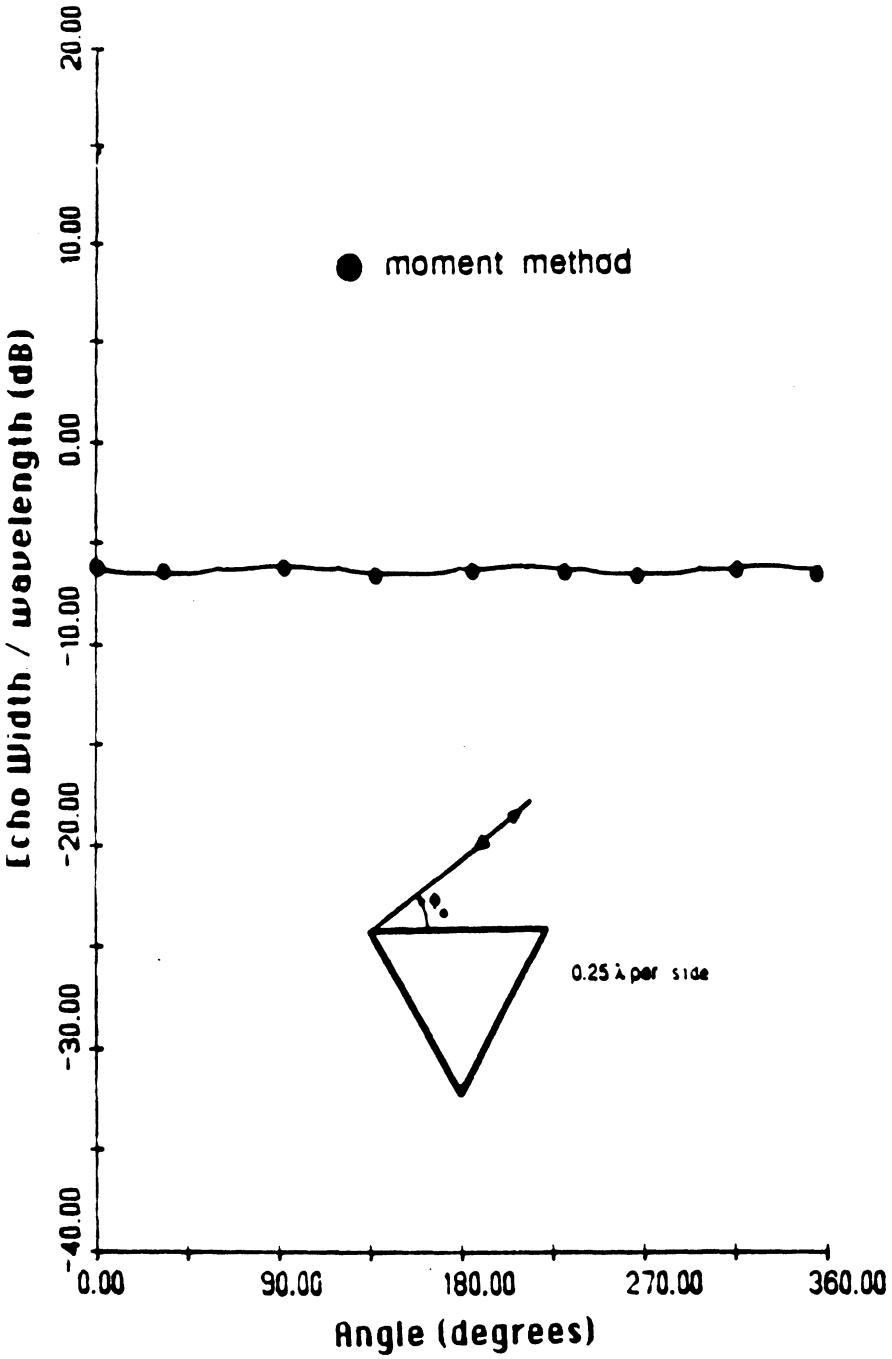
20.00
10.00
0.00
-10.00
-20.00
-30.00
-40.00
Echo Width / wavelength (dB)
moment method
0.25 λ per side
0.00
90.00
180.00
270.00
360.00
Angle (degrees)

20 (f)

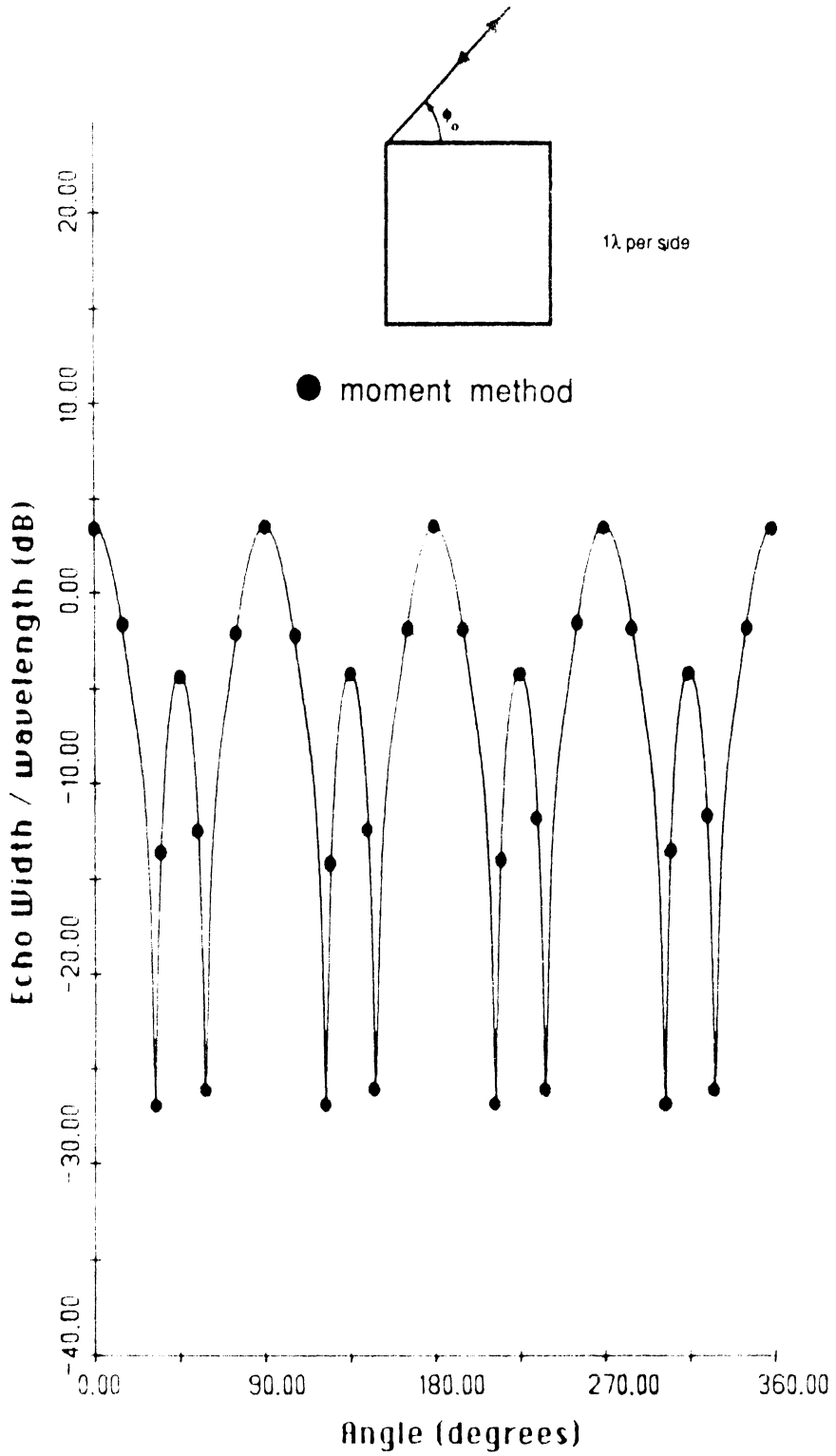

21 (a)

Fig. 21. Comparison of backscatter from an square impedance cylinder with moment method results, E-polarization.
The impedance on all faces is
(a) $\eta = 4$, 1λ in length, and the field consists of single, double, and triple diffraction mechanism contributions,
(b) $\eta = 4$, 1λ in length, single diffraction contribution.

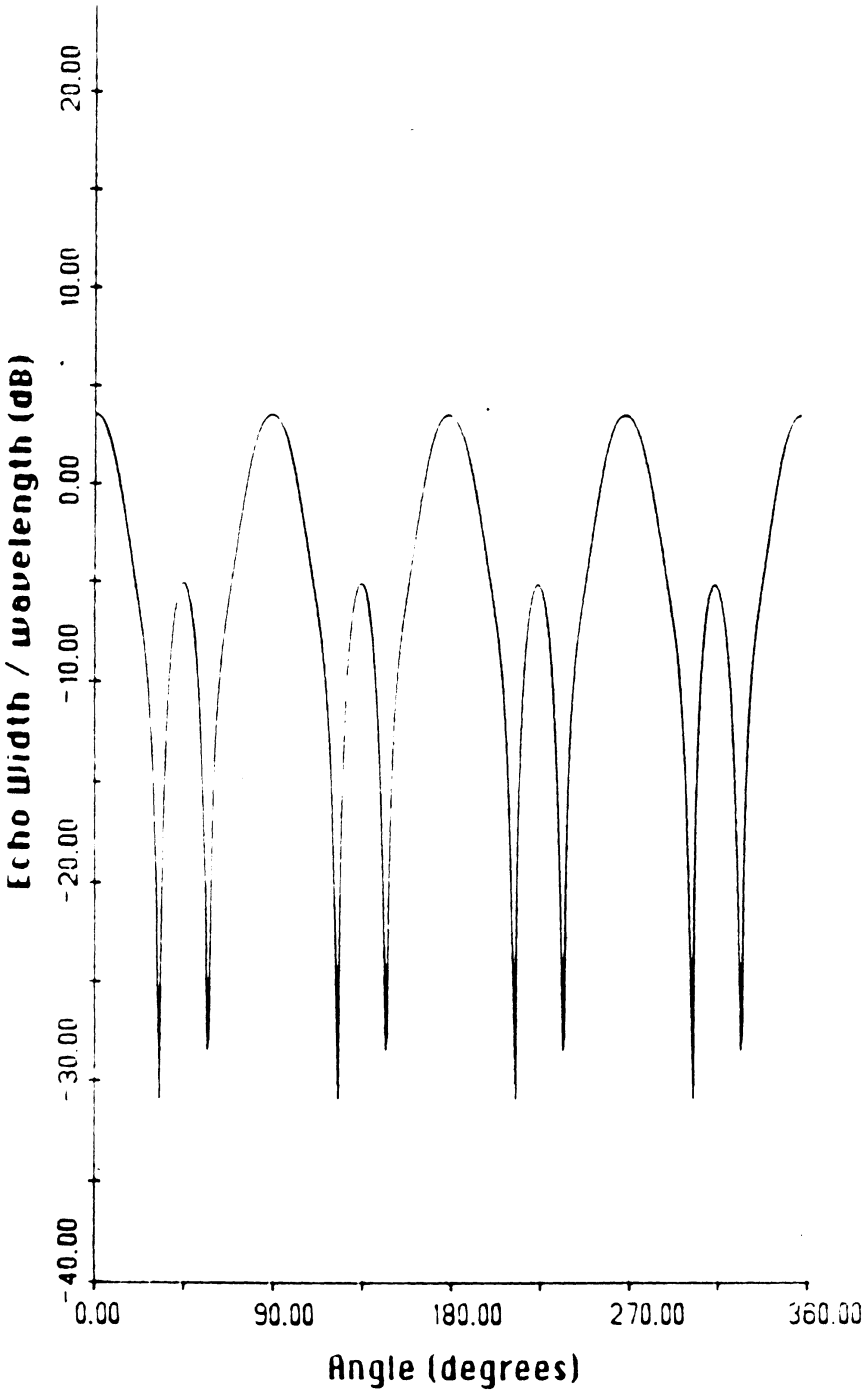
Echo Width / Wavelength (dB)
20.00
10.00
0.00
-10.00
-20.00
-30.00
-40.00
0.00
90.00
180.00
270.00
360.00
Angle (degrees)

21 (b)

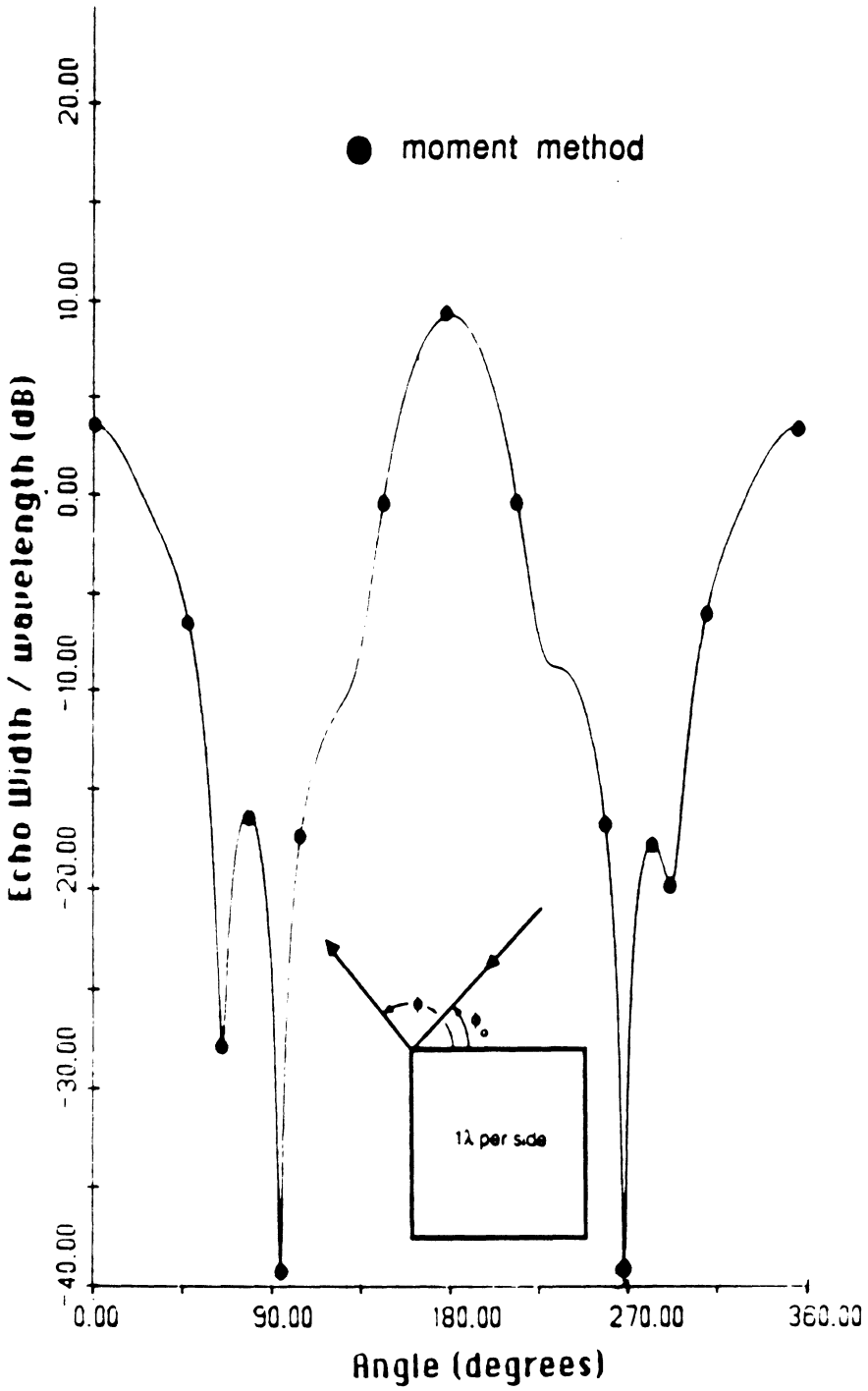

Fig. 22. Comparison of bistatic pattern from an square impedance cylinder with moment method results, E-polarization. The angle of incidence $\phi_o = 1°$. The impedance on all faces is
(a) $\eta = 4$, 1λ in length, and the field consists of single, double, and triple diffraction mechanism contributions,
(b) $\eta = 4$, 1λ in length, single diffraction contribution and
(c) $\eta = 4$, 1λ in length, single and double diffraction field contributions.

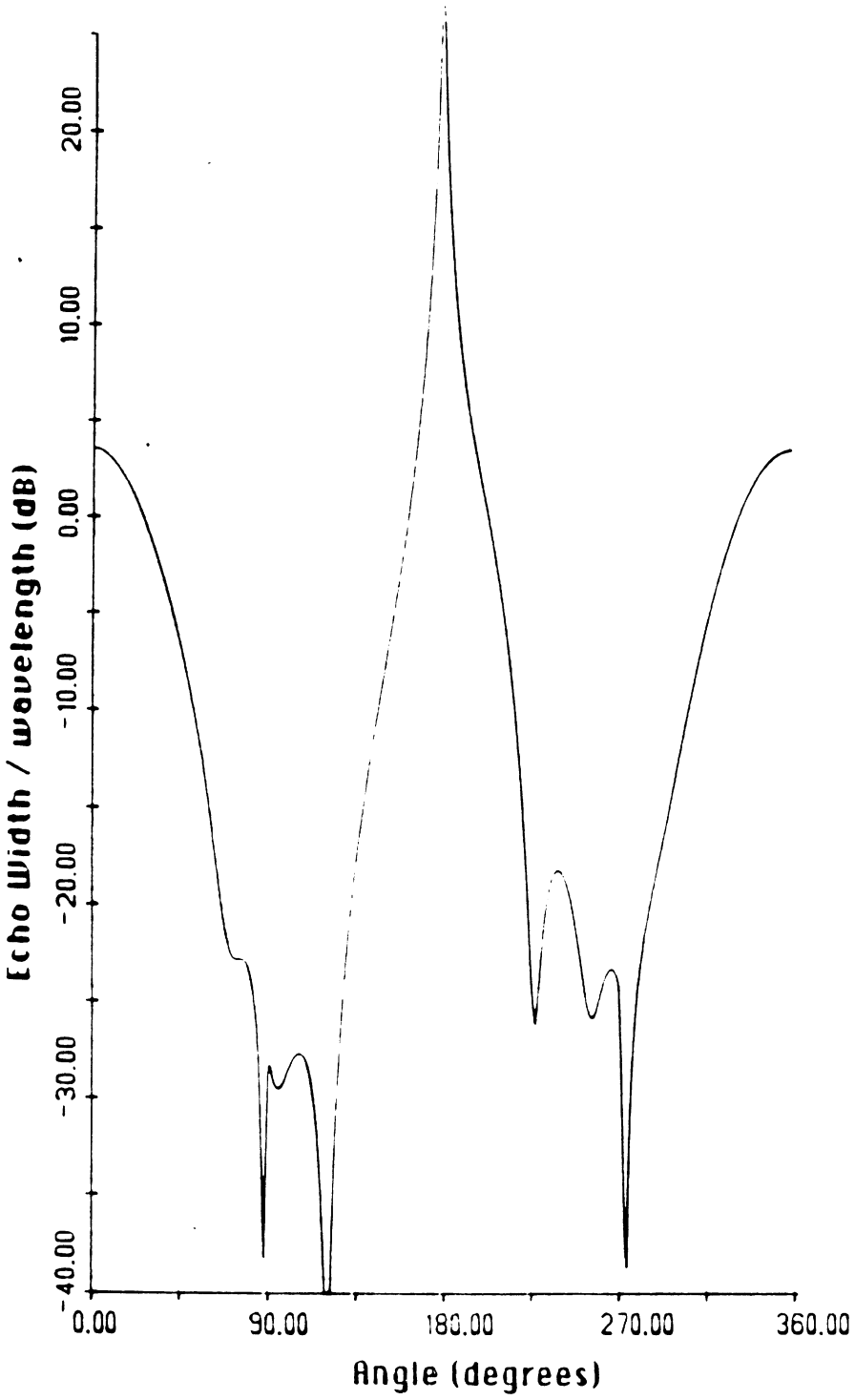
Echo Width / Wavelength (dB)
20.00
10.00
0.00
-10.00
-20.00
-30.00
-40.00
0.00
90.00
180.00
270.00
360.00
Angle (degrees)

22 (b)

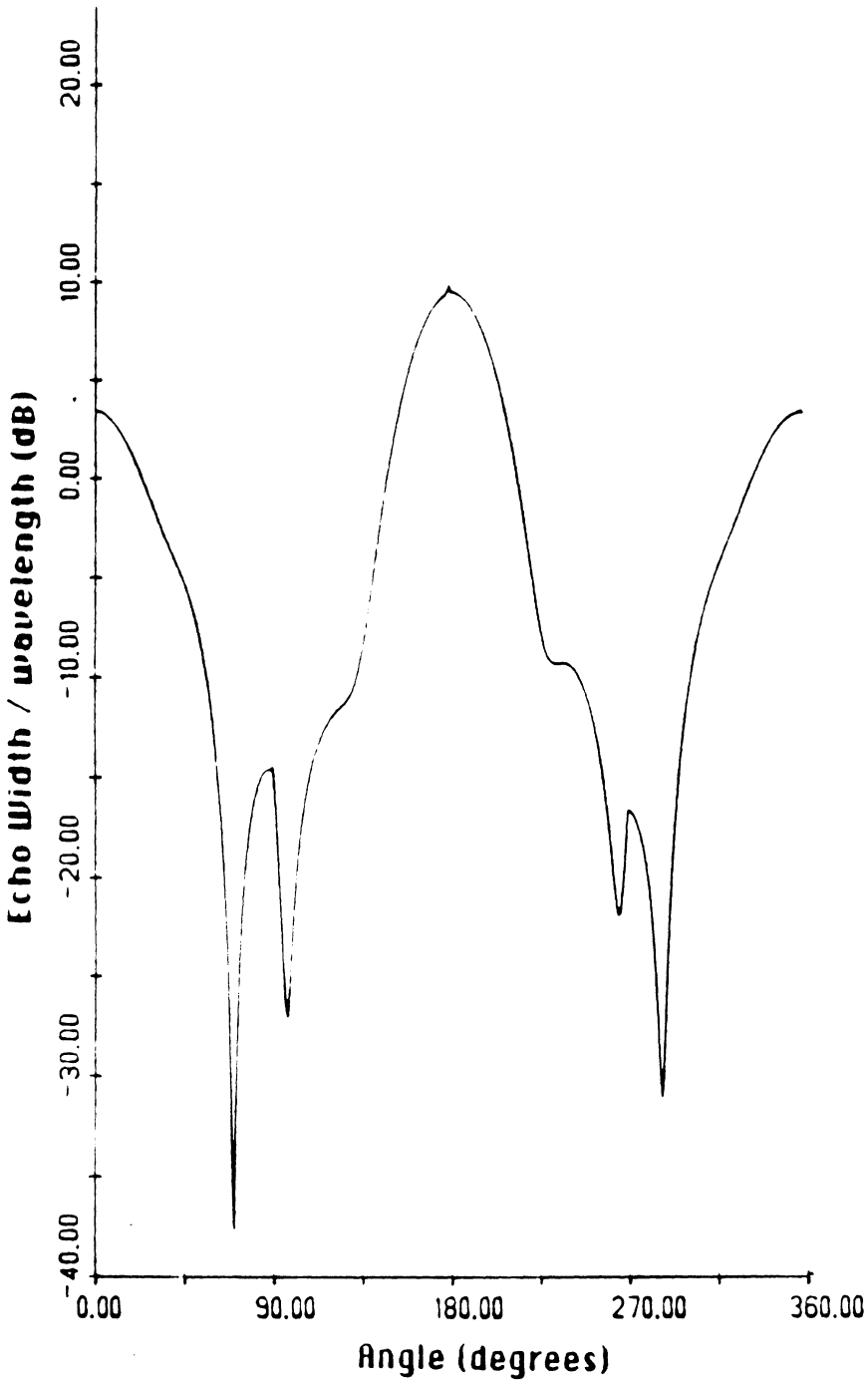
Echo Width / wavelength (dB)
20.00
10.00
0.00
-10.00
-20.00
-30.00
-40.00
0.00
90.00
180.00
270.00
360.00
Angle (degrees)

22 (c)

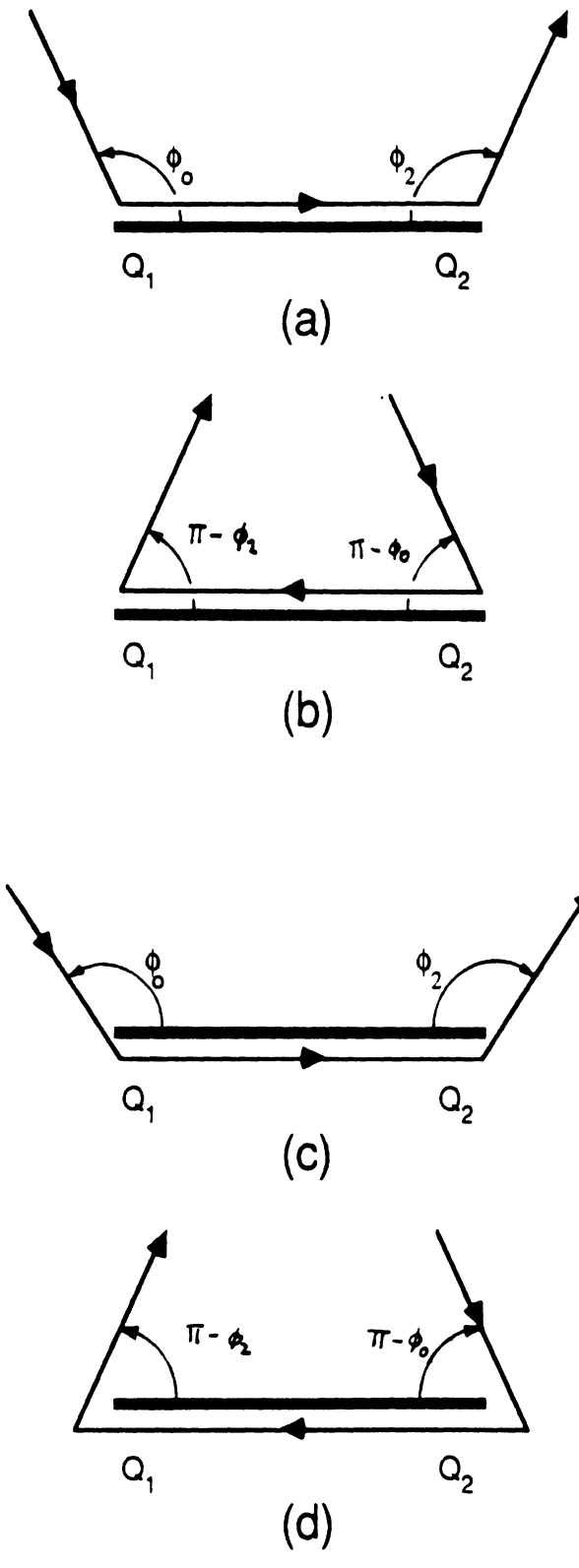

Fig. 23. Double diffraction mechanisms from a strip.

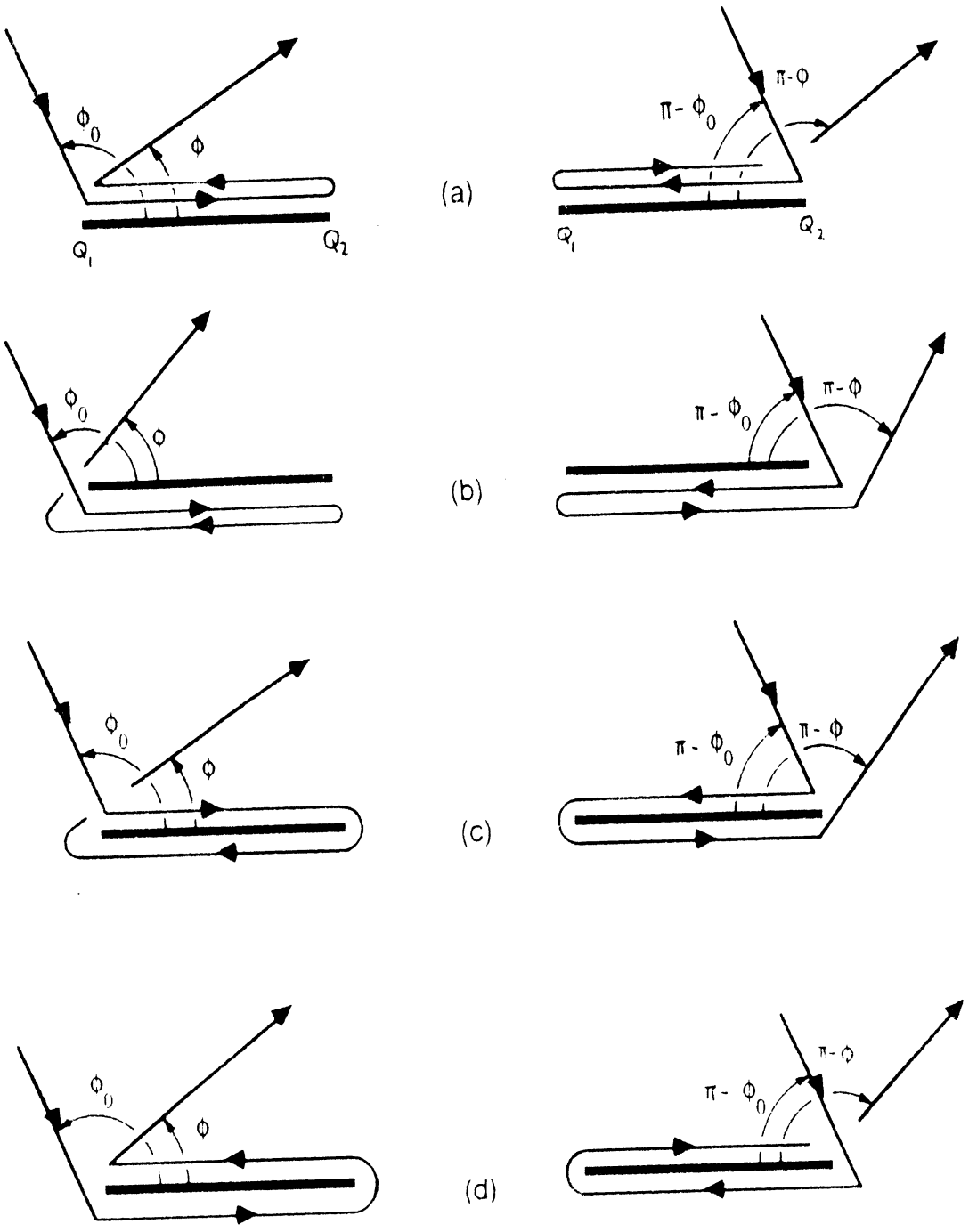

Fig. 24. Triple diffraction mechanisms from a strip.